Macroscopic modelling of arterial traffic: An extension to the Cell Transmission Model

Chaitrali Shirke[a], Ashish Bhaskar[a1], Edward Chung[b]

[a] School of Civil Engineering and Built Environment, Science and Engineering Faculty, Queensland University of Technology (QUT), 2 George St, GPO Box 2434, Brisbane, Qld. 4001, Australia
[b] Department of Electrical Engineering, Hong Kong Polytechnic University, Hung Hom, Kowloon, Hong Kong

Abstract

This paper extends the capability of the cell transmission model (CTM) to capture the complexities of the arterial network. This includes short turning lane blockages and spillbacks, shared lanes, and unbalanced lane utilisation. Moreover, queue estimation accuracy is improved through appropriate consideration of the queue discharge process.

The proposed Arterial Cell Transmission Model (ACTM) has been thoroughly tested with synthetic data and further validated using real data. Compared with the CTM, the proposed ACTM improves the back of the queue estimation accuracy by 20% - 80%. The ACTM offers a more realistic simulation of densities on each lane in case of blockages or spillbacks from short turning lanes and models the interaction among movements in shared lanes including gap acceptance behaviour of permitted turns from shared lanes that are opposed by *through* traffic. The extension also enables the balancing of unequal lane utilisation whenever required. The ACTM is expected to improve the performance of traffic management tools by providing a more realistic simulation of arterial traffic with better queue estimations.

Keywords: Arterial Cell Transmission Model (ACTM); back of the queue (BOQ); short turning lanes; shared lanes; lane utilisation balancing

1. Introduction

Modelling the traffic flow has long been the topic of interest for both researchers and practitioners, and thus various microscopic and macroscopic models are proposed in the literature. The Cell Transmission Model (CTM), proposed by Daganzo (1994), is one of the most widely-used macroscopic models. It is a numerical method to solve differential equations of the LWR model (Lighthill & Whitham, 1955; Richards, 1956) and simulates traffic by evaluating flow at a finite number of carefully selected intermediate points, including the entrance and exit. Compared with microscopic models, the CTM has fewer parameters to calibrate and computationally efficient.

Daganzo (1994) initially proposed the CTM to model traffic on a basic freeway segment. He further applied the model on a freeway network considering merging and diverging behaviours (Daganzo, 1995). Thereafter, Ziliaskopoulos and Lee (1996) extended the traditional CTM for interrupted traffic flow modelling. In addition, researchers (Ziliaskopoulos & Waller, 2000; Avram & Boel, 2005; Kurzhanskiy et al., 2008; Lu et al., 2011; Su et al., 2013) have applied the traditional CTM to simulate traffic on arterial corridors.

Ziliaskopoulos and Waller (2000) developed VISTA (Visual Interactive System for Transportation Algorithms), an independent traffic flow modelling environment based on the traditional CTM. Traffic

---

[1] Corresponding author. Tel.: +61 7 3138 9985; E-mail address: ashish.bhaskar@qut.edu.au

simulation (e.g. AVENUE (Horiguchi et al., 1994)) and signal optimisation software (TRANSYT-13 (Binning et al., 2009)) also use the logic of the CTM or CTM itself for traffic state estimation. For the efficient application of the CTM in signal optimisation, Lo (2001) used CTM as a set of mixed-integer constraints to capture traffic dynamics in mixed-integer linear dynamic signal-control problem. Zhang et al. (2013) showed that the CTM can estimate queues caused by temporal bottlenecks at a network level more realistically as compared to point queue (P-Q) model and the spatial queue (S-Q) model. Furthermore, several studies have used CTM for various applications such as: dynamic traffic assignment, ramp metering, emergency evacuation, and signal optimisation (Lo et al., 2001; Lin & Wang, 2004; Chow & Lo, 2007; Tajtehranifard et al., 2017); short term traffic flow forecasting (Szeto et al. (2009)); pedestrian flow modelling (Iryo-Asano et al., 2007); and model large freeway/arterial/integrated network (Lo & Szeto, 2002; Szeto & Lo, 2004; Van den Berg et al., 2007; Xu et al., 2012; Zhang et al., 2015).

Researchers have introduced several extensions to the traditional CTM to enhance its scope and applicability. Daganzo (1999) proposed a lagged cell transmission model (LCTM) where a lag is introduced in reading the downstream density to enhance the density estimation accuracy of the traditional CTM and it can adopt a non-concave flow–density relation. Following this study, Szeto (2008) showed that the LCTM can yield densities higher than theoretical jam density. To address this limitation, Szeto (2008) proposed improved model, the enhanced LCTM (EL-CTM) by introducing one more term in each sending and receiving function of the model. Unlike LCTM, EL-CTM is proved to yield nonnegative densities not greater than the jam density but still allow the use of non-concave density relations like LCTM. Thereafter, Lu et al. (2011) integrated LCTM with the continuous kinetic models and presented a CTM-based hybrid simulation. This integration accounts for cell density and velocity probability distribution at a cell level. Furthermore, Muñoz et al. (2003) derived switching mode model (SMM) from the CTM to estimate traffic densities at unmonitored locations along a freeway. The SMM switches among different sets of linear differential equations, or modes, depending on the boundary and the congestion status of the cells in a freeway section. Celikoglu (2014) and Celikoglu and Silgu (2016) incorporated the SMM form of the CTM with neural network theory to reconstruct real-time traffic dynamics. Alecsandru (2006); Boel and Mihaylova (2006); (2008); Sumalee et al. (2011) extended the traditional CTM by introducing demand and supply stochasticity in SMM, which is also known as stochastic CTM (SCTM). Work et al. (2008) proposed a velocity-CTM to estimate time-varying traffic density using speed data directly from GPS devices. Chen et al. (2010b) proposed location specific CTM (LS-CTM) for a freeway that can adopt variability in the fundamental diagram along and across a freeway. The LS-CTM incorporates various shapes of the fundamental diagrams to reproduce more complex traffic phenomena such as capacity drops, lane-by-lane variations, nonhomogeneous wave propagation velocities, and temporal lags.

These aforementioned enhancements to the traditional CTM have only been applied/validated for a freeway. However, arterial traffic has complex vehicular interactions with different geometric features (such as short lanes and shared lanes) including interactions at an intersection space and at a traffic control (such as permissive traffic signals) and this requires further modifications in CTM. Researchers have identified following issues in modelling arterial traffic and proposed enhancements in CTM to consider arterial applications:

- Chen et al. (2010a) argued that unlike freeway the trapezoidal fundamental diagram does not truly represent the speed-density relationship of arterial traffic. Hence, for better representation of speed-density relationship on arterials, they have introduced a speed-density table, using query and linear interpolation to relate each density data with a single speed data.

- Arterial traffic merges into different lanes near the stop line depending on the downstream destination (left, through or right). Such behaviour is termed as channelisation. Researchers such as Long et al. (2011); Xie et al. (2013) presented an extended version of the CTM to incorporate the effect of channelisation. Arterial traffic modelling includes modelling of nodes or intersection area in addition to modelling of links. Wang et al. (2012) and Gao et al. (2016) proposed an enhanced CTM to model traffic operations within an intersection area. Wang et al. (2012) proposed a conditional cell transmission model (CCTM) that introduces a conditional cell in the intersection area to capture the behaviour where queue on an arterial link overflows and occupies the intersection area. Furthermore, Gao et al. (2016) presented an enhanced CTM to capture traffic operation at signalised intersections without explicit permissive left-turn yielding rules.
- Hadfi et al. (2017); Tokuda et al. (2017) extended the stochastic CTM for an arterial network by introducing to vehicle agents and their route choice behaviour.
- Researchers (Tuerprasert & Aswakul, 2010; Liu et al., 2015; Tiaprasert et al., 2017) extended the traditional CTM to model multiclass traffic consisting of a mixed composition of vehicle classes. Levin and Boyles (2016a, 2016b) extended the traditional CTM to also model the mixed traffic of manual and autonomous vehicles.
- Non-lane-based heterogeneous traffic is observed on arterial roads in many developing countries such as China, India etc. Kays et al. (2017) extended the traditional CTM for non-lane-based heterogeneous traffic by incorporating a nonlinear fundamental diagram.
- Canudas-de-Wit and Ferrara (2018) proposed Variable-Length cell transmission Model (VLM) and investigated mathematical properties of this model to ensure the consistency with respect to the inherent mass (or vehicle) conservation law.

The above review covers major enhancements in CTM literature. A comprehensive review is beyond the scope of the paper, rather interested readers are refered to Alecsandru et al. (2011) and Adacher and Tiriolo (2018)."

Although abovementioned modifications or extensions (detailed discussion to follow in Section 3) have been suggested to improve the CTM's performance for arterials, the following modelling issues still need to be addressed:

1. *Queue discharge process*: The queue accumulated during signal red time discharges during the signal green time. The flow rate at the stop-line gradually increases to the saturation flow. This gradual increase may be attributed to an initial loss of flow caused by a driver's reaction time and a vehicle's acceleration process. The queue discharge process in the CTM, ignores the initial loss of flow that can result in erroneous capacity estimates.
   The queue discharge process also introduces a backward shockwave. The CTM often fails to identify and model the shockwave effect on arterials (details to follow in Section 3.1). Nevertheless, a realistic modelling of the shockwave effect is crucial for the back-of-the-queue estimation. Traffic on arterial links is highly correlated, and errors in queue estimation on a link can easily propagate to further upstream links. Researchers (Roncoli et al., 2015; Srivastava et al., 2015; Han et al., 2017) have presented modifications in CTM to improve modelling of the queue discharge process. The modelling issues in these studies, and our proposed solution, is discussed in Section 3.1.
2. *Complex geometric configuration*: Geometric configurations, such as short turning lanes and shared lanes, make traffic behaviour and respective modelling complex. A typical example of such complexities is an intersection where traffic is blocked due to such geometric

configurations paired with different demands and signal settings. The most common and under-represented geometric configurations are discussed below.

    a. *Short turning lanes:* Spillback from short *turning* lanes blocks the traffic in adjacent *through* lanes and vice versa. Researchers (Li, 2010; Liu & Chang, 2011) have attempted to model this effect by assuming that spillback occurs when short turning lanes reach the capacity. However, in reality, short *turning* lanes at the capacity do not block adjacent *through* lanes until an additional turning vehicle arrives. Moreover, when the length of a short lane is not a multiple of cell length, it poses a modelling issue, which has not been addressed by previous researchers (more discussion to follow in Section 3.2).

    b. *Shared lanes*: Shared lanes have traffic from multiple turning movements, such as *through* and *right turning*. The interaction between movements in a shared lane, when one of the movements has to give way to opposing *through* traffic or pedestrians, leads to under-utilisation of the shared lane capacity. Hence, the operating characteristics (including the capacity of the shared lane) are significantly different from exclusive lanes. Literature related to the modelling of shared lanes using the CTM is scarce and our understanding on this aspect of modelling remains elusive.

3. *Balancing lane utilisation*: Different lanes may serve the same movements, but their location often leads to an unbalanced lane utilisation. For example, out of two through lanes, one lane located adjacent to a short turning lane can have a higher occupancy due to spillback from the short turning lane. The traditional CTM shows the arterial traffic as movement-by-movement where lanes serving the same movement are modelled as one group. For example, two adjacent lanes serving *through* traffic are modelled together whilst the right (or left) turning lanes are modelled as one group. Therefore, the occupancy difference between two lanes serving the same movement cannot be modelled by traditional CTM. Further, an unbalanced lane utilisation can encourage drivers to change lanes in order to gain the advantage of shorter queues, which is considered as one of the reasons for triggering congestion and more specifically, traffic oscillation. To the best of our knowledge, no previous studies have addressed this lane balancing problem arising from an unequal lane utilisation using the CTM.

In this paper, the CTM is extended to address the aforementioned issues. For the ease of discussion, the proposed model is called the ACTM (Arterial Cell Transmission Model). The rest of the paper is organised as follows: Section 2 describes the traditional CTM; Section 3 introduces the proposed ACTM; followed by the discussion on the calibration for the CTM and ACTM model in section 4 and its thorough testing and validation using synthetic data in section 5; Section 6 applies the ACTM on a real arterial link and its performance is compared with the field observations, and the paper is concluded in Section 7. The notations used hereafter are summarised in Table 1.

Table 1: List of key variables used in the CTM and proposed model formulation

a	Acceptable critical gap
b	Minimum departure headway
dt	Time interval at which cell occupancies are updated in the CTM
L_s	Initial loss time in seconds
$C(L_s)$	Average stop-line detector counts during time L_s seconds
$D_i(t)$	Demand for cell i generated from upstream cell i-1
$D_{i(l) \to i+1(l')}^{LC}$	Lane change demand from cell i of lane l to cell i+1 of lane l'
g	Signal green time in seconds
i	Cell index counting from upstream end of the link (i=1 for upstream most cell)

K_j	Jam density
K_c	Critical density (density that gives maximum flow)
L	Total length of the link modelled in the CTM
L_i	Length of cell i
L_s	Initial loss time
L_{wt}	Distance travelled by shockwave upstream from stop line until time step t
$LC_i^{l\,l'}$	Potential lane changing fraction in cell i at in time step t from lane l to l'
N_i	Maximum number of vehicles a cell i can accommodate at jam density
$n_i(t), n_i^l(t)$	The number of vehicles in cell i (occupancy of cell i) of lane l at time step t
Q_{sat}	Maximum flow (capacity)
$Q_i(t)$	The maximum flow into cell i for time interval $(t, t+1)$
q_l	The flow rate (veh/sec) of the opposing lane l at the intersection
R_i^t , $R_{i(l)}^t$	Receiving capacity of cell i of lane l at time step t
S_i^t	Sending capacity of cell i at time step t
S_{SLR}^t, S_{SLT}^t	Sending capacity of stop-line cell of shared lane for *turning* and *through* movements, respectively at time step t
$S_u(t)$	Saturation flow rate for permitted turn at time step t
t	Time-step index
t_w	Time at which shock wave enters the cell under consideration
V_f	Free flow speed
w	Backward shockwave speed
$y_i(t)$	Inflow to cell i during time interval $(t,t+1)$ (number of vehicles)
$y_{dtotal}(t)$	Total outflow from stop-line cell of shared lane in time interval $(t,t+1)$
$y_{i\rightarrow i+1}(t)$ $y_{i(l)\rightarrow i+1(l)}(t)$	Flow from cell i of lane l to cell $i+1$ of lane l in time interval $(t,t+1)$
$y_{i(l)\rightarrow i+1(l')}^{LC}(t)$	Lane change flow from cell i of lane l to cell $i+1$ of lane l' in time interval $(t,t+1)$
Δ	Minimum headway in opposing traffic
δ , β	Calibration and observed parameter, respectively where $0 < \delta \le 1$ and $0 \le \beta \le 1$
γ_R^t, γ_T^t	Proportion of *turning* and *through* vehicles, respectively
φ_l	Bunching factor for opposing lane l

2 Traditional Cell Transmission Model (CTM)

In the traditional CTM (Daganzo, 1994), a link is divided into homogeneous sections (cells), numbered consecutively from the upstream (i=1) towards the downstream end (i=I) of the modelled road; refer to Figure 1(a). The length of a cell should be more than or equal to the distances travelled under free-flow conditions by a typical vehicle in one clock tick. This is to ensure that the vehicles do not skip a cell. The fundamental diagram for each cell can be approximated as a triangle; refer to Figure 1(b). Equation 1 expresses the number of vehicles, $y_i(t)$, that can flow from cell *i - 1* to cell *i* when the clock advances from *t* to *t + 1*. This equation can be divided into two parts; i.e. sending $S_{i-1}(t)$ (refer to Equation 2) and receiving $R_i(t)$ (refer to Equation 3) capacity of a cell *i-1* and cell *i*, respectively.

5

$$y_i(t) = \min\{n_{i-1}(t), Q_i(t), \alpha(N_i(t) - n_i(t))\} \tag{1}$$
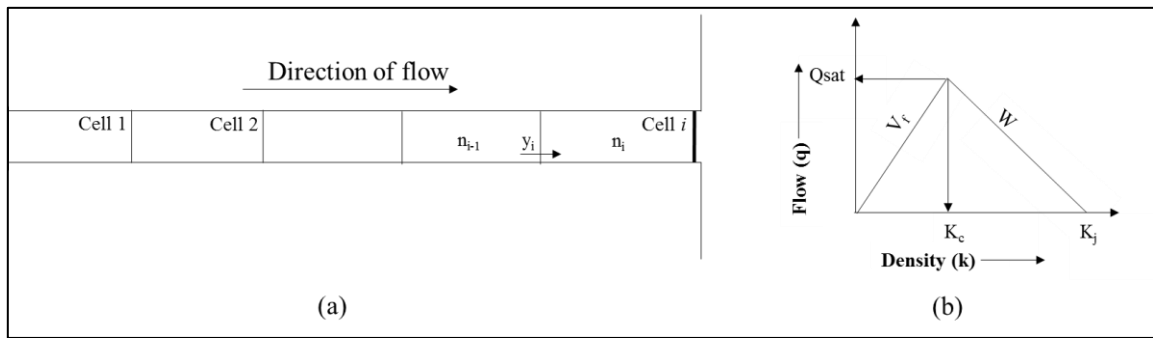
Where, $\alpha = \begin{cases} 1 , & n_{i-1}(t) \leq Q_i(t) \\ \frac{w}{v_f}, & n_{i-1}(t) > Q_i(t) \end{cases}$

$$S_{i-1}(t) = min\{n_{i-1}, Q_i(t)\} \tag{2}$$

$$R_i(t) = \min\{Q_i(t), \alpha(N_i(t) - n_i(t))\} \tag{3}$$

Further, cell occupancy is updated for each time interval. Here, occupancy (n_i) of cell i at time step $t +$ 1 equals its occupancy in time step t, plus the inflow from cell i-1, and minus the outflow to cell $i+1$; i.e.

$$n_i(t + 1) = n_i(t) + y_i(t) - y_{i+1}(t) \tag{4}$$

Figure 1: (a) Network representation of the CTM; (b) Triangular fundamental diagram

The above set of equations represents the CTM model that was initially developed for freeways. The ensuing section provides insights into the applicability of the traditional CTM on arterial networks, discusses the modifications proposed in the literature for the CTM's applicability on the arterial network, and presents the proposed ACTM.

3 Modelling arterial traffic with the CTM

This section presents the details of the proposed ACTM that introduces modification in the traditional CTM to realistically capture the queue discharge process (Section 3.1); and extends the CTM to capture: 1) interactions among different movements causing lane blockages or spillbacks at short turning lanes (Section 3.2); 2) interactions at shared lanes (Section 3.3); and 3) interactions among lanes arising from unbalanced lane utilisation (Section 3.4).

For the proposed ACTM, we model each lane separately. In general, for the arterial network, we recommend modelling each lane separately especially when short lanes or shared lanes are present. However, if needed, the lanes serving the same movement can be grouped together. For instance, if there is no significant difference in the utilisation of lanes serving the same movements, then those lanes can be grouped together, except the lane adjacent to a short lane or shared lane.

3.1 The ACTM for queue discharge process

3.1.1 Start-up loss

A typical queue discharge profile in the traditional CTM is illustrated in Figure 2 (a), where at time=0, the signal turns green and the vehicles queuing behind the stop line start discharging at saturation flow

rate until the queue is served or the traffic light turns red. It has been frequently observed that start-up acceleration of vehicles causes capacity loss, due to which the discharge flow rate at a stop line gradually increases from zero to saturation flow rate as shown in Figure 2(b) (Webster, 1958). To account for this gradual change, Srivastava et al. (2015) introduced a modified demand function by adding a new variable, called 'jam demand'; i.e. the demand at the jam density that linearly decreases in density for congested conditions. Demand at the jam density adds to the calibration of parameters. The headway and discharge flow rate profiles obtained through this function provide qualitatively better representations of the expected shapes of curves.

For real-time applications, we propose another simpler approach by introducing a step profile for the queue discharge flow rate; refer to Figure 2(c). Here, flow rate (q) is modelled as a proportion of the saturation flow rate (δQ_{sat}) for the initial loss time L_s and saturation flow rate thereafter (refer to Equation 5).

$$q(t) = \begin{cases} \delta Q_{sat}, & t < L_s \\ Q_{sat}, & t \geq L_s \end{cases} \tag{5}$$

The value of δ can be obtained using the stop-line detector counts as follows:

$$\delta = \frac{C(L_s)}{Q_{sat} * L_s} \tag{6}$$

Where $C(L_s)$ is the average stop-line detector count during L_s, the value of L_s can be obtained from the field observations and it usually varies from 2 to 5 seconds (Akçelik et al., 1999). For modelling, it is recommended to approximate the value of L_s as a multiple of the simulation time step. Based on our real world experiment (detailed in Section 6), we recommend the default value of δ as 0.5.
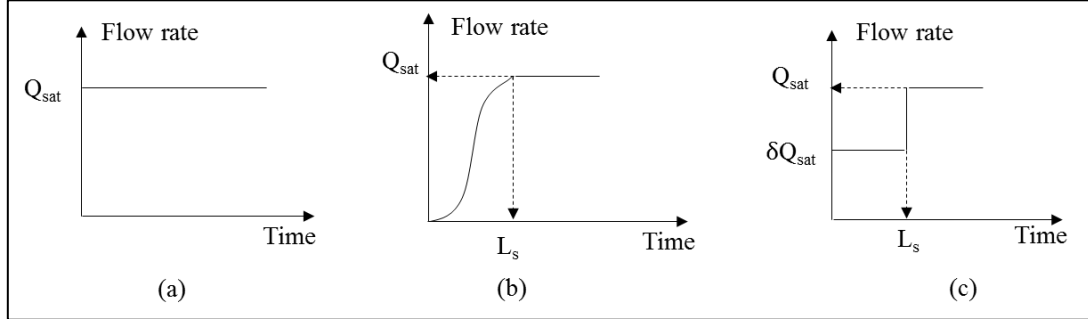

Figure 2: Discharge flow rate for the CTM (a) without lost time; (b) with start-up lost time; and (c) proposed discharge flow profile

3.1.2   Shockwave effect

The real behaviour of traffic flow during the queue discharge process can be explained with the help of Figure 3, where vehicle trajectories during a signal cycle are presented. The horizontal-axis and vertical-axis represent the time and space, respectively. The time-space region is divided into rectangular grids with dimensions of the simulation time step (along x-axis) and the cell size (along y-axis). Here, the signal turns green during time interval t_x and a backward shockwave with the speed w, which is less than the free-flow speed that enters the cell i (as shown by the arrow). During the time interval t_x, the cell i has reached jam density and vehicles from the upstream cell cannot flow into the cell i until the time interval t_{x+5} when the shockwave travels out of the cell i. Similarly, in the current example, cell i -1 is at jam density when the shockwave enters the cell during time interval t_{x+5} and vehicles cannot flow into cell i-1 until the shockwave leaves the cell during time interval t_{x+10}. However, the density of the cell i-2 is lower than jam density at the time when the shockwave enters the cell (during time interval

t_{x+10}). Therefore, entry flow in cell *i-2* will not be zero, even when the shockwave is traveling into the cell *i-2*. Note that if the backwards shockwave speed is equal to the free-flow speed and the cell length is equal to the distance travelled under free flow condition by a vehicle in one clock tick then the vehicles from cell *i-1* can move into cell *i* at time step t_{x+1}. However, in real world backward shockwave speed is less than free-flow speed.
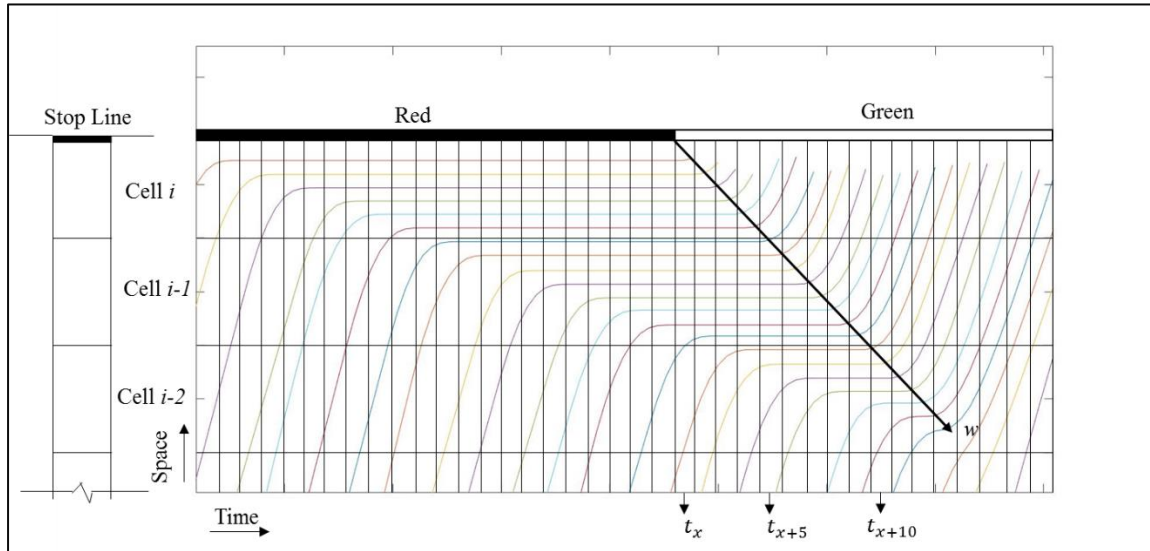
Figure 3: An example for the shockwave effect at signalised an arterial intersection

From the above illustration (Figure 3) it can be concluded that, if a cell *i* is at jam density during queue discharge then the vehicles from the immediate upstream cell *i-1* cannot flow into the cell *i* until the last vehicle in the cell *i* has moved forward from its stopping position; i.e. the shockwave has moved out of cell *i*.

Interestingly, the traditional CTM models the supply of the cell considering homogeneous density within the cell and ignores that the queue starts discharging from the front of the cell and back of the cell contains queued vehicles as described above.

Researchers (Roncoli et al., 2015; Srivastava et al., 2015; Han et al., 2017) have addressed the above issue by incorporating capacity drop phenomenon, where generally the demand function is modified to reduce the flow into cell *i* using the assumption that when the density of a cell *i-1* is beyond the critical value, the demand decreases linearly with increasing density. Using this approach, Roncoli et al. (2015) presented an optimisation-oriented first-order model to model capacity drop on freeways, whereas Srivastava et al. (2015) used a similar approach to capture the initial headway behaviour for urban traffic as discussed in Section 3.1.1.

Han et al. (2016) tested the above models for the freeway stretch and showed that the above-mentioned models considered only the standing queue and therefore cannot reproduce the propagation of shockwaves accurately. Further, to take into account the propagation of shockwaves on the freeway network, Han et al. (2017) revised the supply function that depended on density difference between cell *i* and its upstream cell *i-1,* where both cells are congested. However, on arterial links where the shockwave is generated during each cycle, if the upstream is in free-flow condition, as per Han et al. (2017)'s modification, the demand function of the targeting cell will have the same structure as the traditional CTM and it will overestimate the real discharge rate in the targeting cell.

Hence, to correctly model the effect of the shockwave in each cell, as demonstrated in Figure 3, the following solution is proposed: during queue discharge, vehicles should not be allowed to flow into the downstream cell if: a) the density of the cell reaches jam density before or during queue discharge, and b) the shockwave is present within that cell. After the shockwave has crossed the cell, flow into the cell during the following time intervals will be as per the traditional CTM. For this, the flow equation of the CTM (i.e. Equation 1) is modified into Equation 7.

$$y_i(t) = \begin{cases} 0, & if \ n_i(t_w) \geq N_i \cap (L - \sum_{x=1}^{i-1} L_x) > L_{wt} \geq (L - \sum_{x=1}^{i} L_x) \\ \min\{n_{i-1}(t), Q_i(t), (N_i(t) - n_i(t))\}, & Else \end{cases} \quad (7)$$

Where,

- L_{wt} represents the distance travelled upstream by the shockwave from the stop line until the current time *t*.
- $n_i(t_w) \geq N_i$ represents the density of cell *i* is equal to jam density as the shockwave enters it ; and
- $(L - \sum_{x=1}^{i-1} L_x) > L_{wt} > (L - \sum_{x=1}^{i} L_x)$ represents the shockwave is travelling within the cell *i* during the time interval *t*. This condition is true when L_{wt} is less than the distance of the upsteam end of the cell *i* from stop line; i.e. $(L - \sum_{x=1}^{i-1} L_x)$, and greater than or equal to the distance of the downstream end of the cell *i* from stop line *i.e.* $(L - \sum_{x=1}^{i} L_x)$.

3.2 The ACTM for the short lane

For ease of the explanation, refer to the example illustrated in Figure 4. Here,

- The queue on the adjacent lane can block the inflow into the short lane (see Figure 4(a)); or the short turning lane can spill back and block the adjacent lane (see Figure 4(b)). Such scenarios lead to an under-utilisation of the lanes' capacity.
- Figure 4(c) demonstrates the case where the short turning lane reaches its capacity; however, it does not block the flow in the adjacent *through* lane. In this case, the short turning lane is utilised 100% without affecting the capacity of the adjacent lane.

To accurately analyse the performance of arterial traffic, it is important to simulate these cases that arise due to interaction among various movements. For example, if the case of a short lane at capacity is overlooked while modelling interactions, delay to the adjacent through lane will be overestimated.

Another challenge in modelling the short lane arises when the length of the short turning lane is not a multiple of the modelled CTM cell length; i.e. one of the cells in the short lane has a shorter length than the modelled cell length: similar to the example presented in Figure 4(d). Cell length for the CTM is modelled according to the distance travelled under free-flow speed by a vehicle in one simulation time step. For a selected simulation time step it is possible that all short turning lanes cannot be divided into an integral number of cells. This situation can be avoided by reducing the simulation time step such that the required minimum cell length is equal to the shortest short lane length in the network. However, smaller simulation time steps will result in increased computation time and might not be suitable for a long corridor or large network. Therefore, we propose an approach that should not restrict the modelling to a short time step, and should correctly model short lane blockages and spillbacks for scenarios with cell size in the short lane less than the desired cell size (as shown in Figure 4(d)).
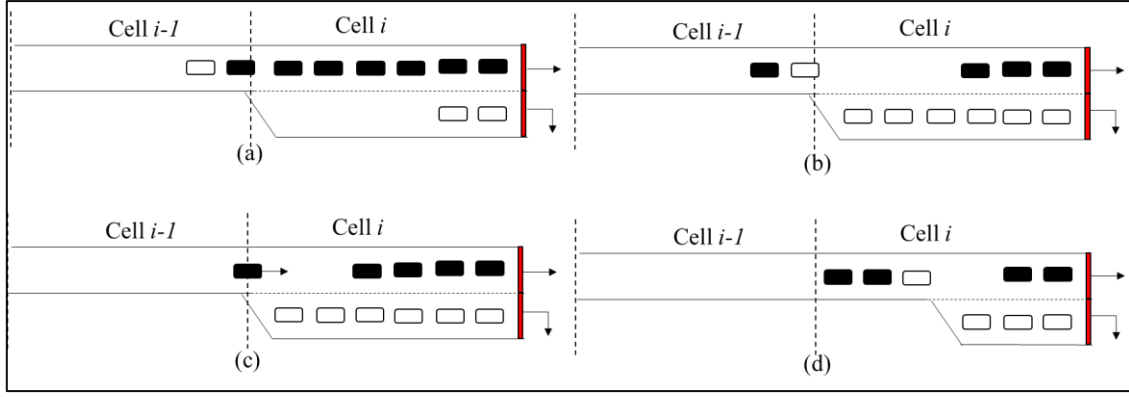
Figure 4: (a) Short lane blockage; (b) Short lane at capacity; (c) Spillback from short lane; and (d) Short lane length less than cell length. The vertical dash line represents the boundary of the cell; the black rectangles are *through* vehicles and the white rectangles are *right turning* vehicles.

The short lane modelling issue in the traditional CTM is discussed below, followed by a new approach to address it.

Refer to Figure 5(a) where the *through* lane with a short lane for a right turn (left-hand driving) is presented. In general, for modelling the link with the short lane, each lane is divided into cells of equal lengths and categorised into three zones from the stop line, namely, the *channelised zone*, the *gate cell*, and the *progression area*. The *channelised zone* refers to an area where vehicles diverge into their target lanes *through* or *turning*. The *gate cells* are cells in each lane that are immediately upstream of the *channelised zone*. The remaining part of a link belongs to the *progression area*.

We named the channelised cell of the short *right turning* lane, adjacent *through* lane, and the cell immediately upstream of it, as 'R', 'T' and 'G', respectively. The cells in the progression area are numbered from 1 to I, starting from the upstream end of the link for each lane.

Researchers (Li, 2010; Liu & Chang, 2011) have modelled aforementioned interactions among movements at the short lane using the diversion equation of the CTM (Daganzo, 1995), where total outflow from the gate cell G is calculated by Equation 8 and this outflow is distributed into cell R and T using Equations 9 and 10, respectively.

$$y_{G \to R\&T}(t) = \min\left\{ S_G^t, \frac{R_R^t}{\gamma_R^t}, \frac{R_T^t}{\gamma_T^t} \right\} \tag{8}$$

$$y_{G \to R}(t) = y_{G \to R\&T}(t) \times \gamma_R^t \tag{9}$$

$$y_{G \to T}(t) = y_{G \to R\&T}(t) \times \gamma_T^t \tag{10}$$

In Equation 8, $y_{G \to R\&T}(t)$ represents the number of vehicles flowing out from cell G, which is the minimum of the sending capacity of cell G (S_G^t), the right-turn receiving capacity ($\frac{R_R^t}{\gamma_R^t}$), and the *through* receiving capacity ($\frac{R_T^t}{\gamma_T^t}$). Here, γ_R^t and γ_T^t present proportion of *turning* and *through* vehicles respectively. According to these equations, if actual receiving capacity of cell R i.e. $R_R^t = 0$ then $y_{G \to R\&T}(t) = y_{G \to T}(t) = 0$. As a result, the flow into the adjacent *through* cell (T) will be zero once the *turning* cell (R) has reached it capacity, without considering whether the next incoming vehicle is *through* or *turning*. This diversion operation overlooks the case of the short lane at capacity (refer to Figure 4(b)).

The above diversion operation also fails to correctly model the case where the cell in the short lane has a smaller length than the adjacent cell (*see* Figure 4(d)). Here, when the short lane cell reaches capacity (i.e. $R_R^t = 0$), the outflow from cell G should be zero (as per Equation 8, $y_{G \to R\&T}(t) = 0$). However, in reality, $y_{G \to R\&T}(t) \neq 0$ because there will still be space for *through* and *right turning* vehicles in cell T after the short lane spillback or blockage.
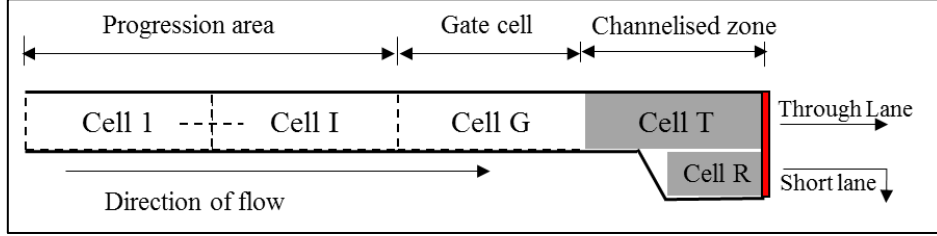
(a) Cell Arrangement in the case of the short lane
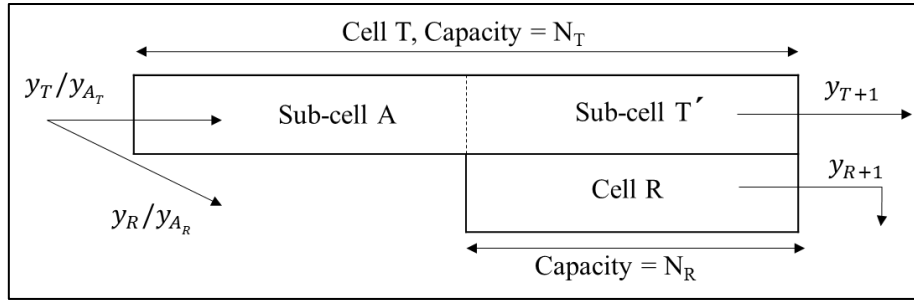
(b) Capacity distribution of cell T
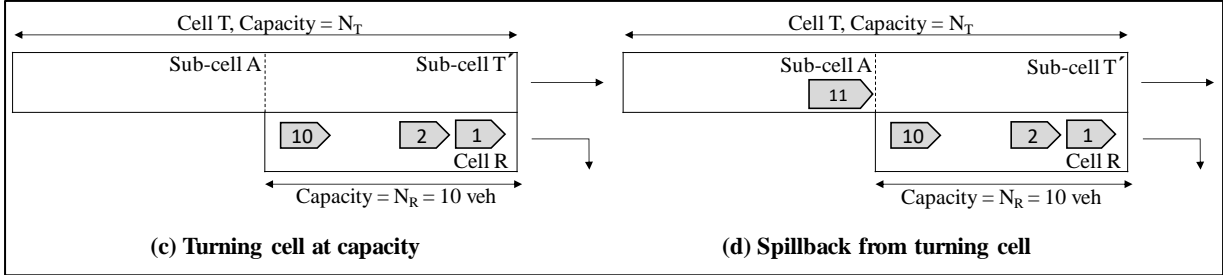
(c) Turning cell at capacity   **(d) Spillback from turning cell**

Figure 5: Proposed set up for the CTM in the case of the short turning lane

The above issues are addressed in the ACTM where we propose modifications to calculate the flow of vehicles to and from cell T and cell R. For ease of explanation, refer to Figure 5(b) where the T is virtually bifurcated into sub-cell A and T′ such that sub-cell T′ and cell R are of the same size. Let the actual capacities of cell R and T be N_R and N_T, respectively, such that $N_R < N_T$.

For ease of modelling the capacities of cell R and sub-cell T′ are set to $N_R + 1$ and not N_R. Here, the blockage occurs when there is spill over from the short lane (R) or adjacent *through* cell (T′). The spill over can be represented by the 'N_R+1'th vehicle demand for the short lane. To consider this effect, one can either a) consider the capacity of the short lane as the actual capacity (N_R) and keep track of the demand from sub-cell A for short lane or b) virtually increase the capacity of the short lane by one, i.e., consider the capacity of cell R as 'N_R+1' and model the spill over once the cell has reached this value. For ease of modelling we have considered the latter case. To further explain this adjustment, consider Figure 5(c) and Figure 5(d) where the actual capacity of the short lane is 10 vehicles. When the occupancy of the short lane has reached 10 vehicles there is still scope for flow into through lane (Figure 5(c)) from sub-cell A to sub-cell T, until the arrival of 11th vehicle for short lane (Figure 5(d)). From this we can say that when occupancy of either cell R or sub-cell T' exceeds N_R, vehicles cannot flow into cell R and sub-cell T′ IE $y_{G \to T'}(t)$ and $y_{G \to R}(t)$ should be zero.

From the above, the capacity of sub-cell A is modelled as ($N_T - N_R - 1$). Sub-cell A carries traffic for both *through* and *right turning* vehicles, whereas sub-cell T′ has only *through* traffic. Once cell R or T′ exceeds capacity, further inflow into cell T is stored into sub-cell A. The sub-cell A is virtually divided into A_T and A_R, which stores the *through* and *right* traffic from sub-cell A to sub-cell T and R, respectively. The variable $y_{G \to A_T}$ and $y_{G \to A_R}$ represents the flow from cell G to the sub-cell A_T and A_R, respectively. The variable n_{A_T} and n_{A_R} represents the demand from sub-cell A towards sub-cell T′ and R, respectively. Total occupancy of sub-cell A is the sum of n_{A_T} and n_{A_R}.

Vehicles stored in sub-cell A will not move out until occupancy of sub-cell T′ and cell R is less than or equal to N_R, which means the short lane blockage or spillback is cleared. Note that if the short lane length is multiples of cell length, then sub-cell A will not exist, but the proposed modelling procedure will still be able to correctly model the short lane spillback, blockage and short lane at capacity.
The above procedure can be implemented using the following set of equations:

1. Calculate inflow in T', R and A

    IF $n_R(t) \leq N_R$ AND $n_{T'}(t) \geq N_R$: *Short lane blockage* $\qquad$ (11)

    $$y_{G \to A}(t) = \min\left(S_G^t, Q_T(t), N_T - n_{T'}(t) - n_{A_T}(t) - n_{A_R}(t)\right)$$

    $$y_{G \to A_R}(t) = y_{G \to A}(t) \times \gamma_R, \ y_{G \to A_T}(t) = y_{G \to A}(t) \times \gamma_T$$

    $$y_{G \to T'}(t) = y_{G \to R}(t) = 0$$

    OR IF $n_R(t) > N_R$ AND $n_{T'}(t) < N_R$: *Short lane spillback* $\qquad$ (12)

    $$y_{G \to A}(t) = \min\left(S_G^t, Q_T(t), N_T - n_R(t) - n_{A_T}(t) - n_{A_R}(t)\right)$$

    $$y_{G \to A_R}(t) = y_{G \to A}(t) \times \gamma_R, \ y_{G \to A_T}(t) = y_{G \to A}(t) \times \gamma_T$$

    $$y_{G \to T'}(t) = y_{G \to R}(t) = 0$$

    OR $\quad$: *No short lane spillback or blockage* $\qquad$ (13)

    $$y_{G \to T'}(t) = \min\left(S_G^t \times \gamma_T, \ Q_T(t) \times \gamma_T, \ (N_R + 1) - n_{T'}(t)\right)$$

    $$y_{G \to R}(t) = \min(S_G^t \times \gamma_R, \ Q_T(t) \times \gamma_R, \ (N_R + 1) - n_R(t))$$

    $$y_{G \to A_R}(t) = y_{G \to A_{T'}}(t) = 0$$

2. Calculate the outflow from cell T' and R into respective downstream cells, say cell $T+1$ and $R+1$

    IF $n_{T'}(t) > N_R$ OR $n_R(t) > N_R$, $\qquad$ (14)

    $$y_{T' \to T+1} = \min(n_{T'}(t), \ Q_{T+1}(t), \ N_{T+1} - n_{R+1}(t))$$

    $$y_{R \to R+1} = \min(n_R(t), \ Q_{R+1}(t), \ N_{R+1}(t) - n_{R+1}(t))$$

    OR $\qquad$ (15)

    $$n_{T'} = n_{T'} + \min(n_{A_T}, (N_R + 1) - n_{T'}(t))$$

    $$n_{A_T} = n_{A_T} - \min(n_{A_T}, (N_R + 1) - n_{T'}(t))$$

    $$y_{T' \to T+1} = \min(n_{T'}, \ Q_{T+1}, \ N_{R+1} - n_{R+1})$$

    $$n_R = n_R + \min(n_{A_R}, (N_R + 1) - n_R(t))$$

    $$n_{A_R} = n_{A_R} - \min(n_{A_R}, (N_R + 1) - n_R(t))$$

    $$y_{R \to R+1} = \min(n_R, \ Q_{R+1}, \ N_{R+1} - n_{R+1})$$

The proposed procedure allows us to realistically model all three cases of interaction among movements even when the short lane length is not a multiple of cell lengths as demonstrated in Figure 6. All the possible occupancies of cell R and T′ are identified, and the corresponding equations to calculate inflow and outflow are mapped in Figure 6.
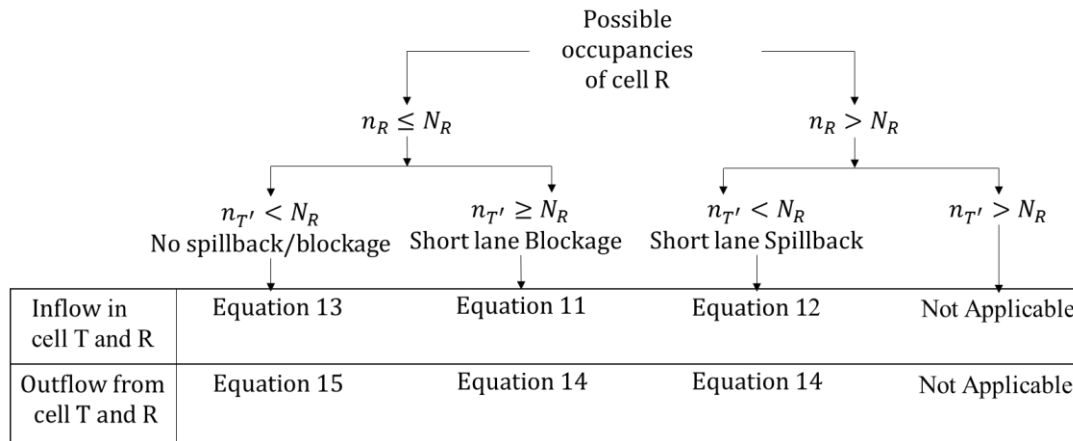
**Figure 6: Combination of cell occupancies in the presence of the short turning lane**

The above equations assume that $N_R > Q_{sat} \times dt$. When this assumption is not true, the time interval dt can be reduced or the aforementioned equations can be further modified. To avoid unnecessary confusion these modifications are outside the scope of this paper.

3.3 The ACTM for shared lane modelling

For a realistic simulation of a shared lane, interaction of different movements sharing the same lane (where one of the movements can block the other) need to be incorporated. For example, the *through* movement can get blocked when it shares the lane with a *turning* movement with a permitted turning phase against the opposing traffic. Here, the turning traffic generally has an interrupted flow during the permissive green due to the lack of an acceptable/safe gap in the opposing traffic. Such blockages reduce the capacity of a shared lane as compared to exclusive lanes. Therefore, it is important to treat shared lanes differently from exclusive lanes.

One of the pioneering analytical models that estimate the capacity of shared lanes was proposed by Akcelik (1988). Along similar lines, researchers (Xu et al., 2008; Creasey et al., 2011; Wu, 2011; Zhou & Zhuang, 2011; Chen et al., 2014) have proposed analytical models to estimate the capacity of a shared lane under various scenarios, such as vehicles allowed to *turn on red* and share the lane with *through* vehicles; a *permitted turning* phase for a shared lane; a shared lane with an additional waiting area for *turning* movements within intersection; interaction of a *permitted turn* in a shared lane with pedestrians, etc. Most of these analytical models aggregate the impact of opposing traffic (an acceptable/safe gap in opposing traffic) on the capacity of a shared lane. If the impact of the opposing traffic on shared lane traffic is introduced in the CTM it should capture varying capacities of a shared lane. To our knowledge, no dedicated effort exists in the literature to model shared lanes using the CTM, and this paper addresses this gap; the details for which are presented below.

The uniqueness of the proposed modelling of the shared lane using the CTM and the modelling of the exclusive lane is in the calculation of the outflow from the stop-line cell of a shared lane. Figure 7 demonstrates the arrangement of cells and nomenclature followed hereafter. The stop-line cell of a shared lane is referred to as SL, and the first cells in the downstream *through* and *turning* lanes are referred to as dT and dR, respectively. Note, for ease of explanation we consider *right turning* (left-hand driving) as the turning movement.
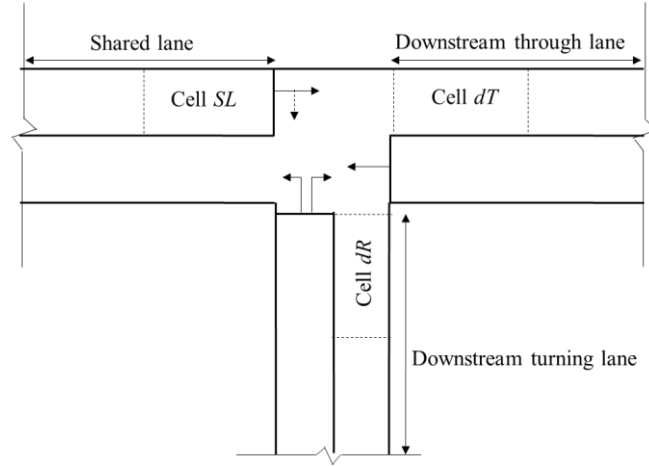
Figure 7: Arrangement of cells for the shared lane model

The two most common scenarios of a shared lane are: a) leading or lagging turning phase; and b) permitted turning phase. The following presents the corresponding calculations of stop-line flow at a shared lane for the CTM.

(a) *Turning* and *through* movements share the lane and both receive right-of-way during different phases; e.g. leading or lagging turning phases.

When *turning* vehicles receive right-of-way before *through* vehicles or vice versa, the movement that receives right-of-way can depart the stop line freely until a vehicle of another movement arrives at the stop line. Hence, we adopted the following formula from Akcelik (1988) to calculate the demand of the movement that receives right-of-way at the beginning of every cycle.

$$S_{SLR}^t = \begin{cases} \dfrac{\gamma_R^t}{\gamma_T^t}(1 - \gamma_R^{t\ M}), & \gamma_T^t > 0 \\ \\ M, & \gamma_T^t = 0 \end{cases} \tag{16}$$

$$S_{SLT}^t = \begin{cases} \dfrac{\gamma_T^t}{\gamma_R^t}(1 - \gamma_T^{t\ M}), & \gamma_R^t > 0 \\ \\ M, & \gamma_R^t = 0 \end{cases} \tag{17}$$

$$M = Q_{sat} * g \tag{18}$$

Where *M* represents the maximum number of blocked departures for a respective movement, which is a product of the saturation flow rate (Q_{sat}) – expressed in vehicle/second – of a movement being blocked and green time (g) of the phase serving that movement. γ_R^t and γ_T^t represent the proportion of *right turning* and *through* vehicles in cell SL, respectively. S_{SLR}^t and S_{SLT}^t are the demand of *right turning* and *through* vehicles, respectively, which can depart the stop line before getting blocked by other movements during respective phases. Once this demand is satisfied during a given green time for a movement, the flow out from a shared lane will be zero due to a blockage for the remaining green time, if any.

Every time a signal turns green for a *turning* movement, S_{SLR}^t is set equal to the value obtained from Equation 16, which is updated for succeeding time intervals using Equation 20. The outflow of *turning* vehicles from the stop-line cell of a shared lane at each time interval *t*, i.e. $y_{dR}(t)$, is calculated using Equation 19 where R_{dR}^t represent receiving capacity of downstream cell for *right turning* traffic.

14

$$y_{dR}(t) = \min(S_{SLR}^t, Q_{sat}, R_{dR}^t) \tag{19}$$

$$S_{SLR}^{t+1} = \min(0, S_{SLR}^t - y_{dR}(t)) \tag{20}$$

Similarly, in each cycle when the signal turns green for a *through* movement, the following equations are used:

$$y_{dT}(t) = \min(S_{SLT}^t, Q_{sat}, R_{dT}^t) \tag{21}$$

$$S_{SLT}^{t+1} = \min(0, S_{SLT}^t - y_{dT}(t)) \tag{22}$$

(b) *Turning* and *through* movements share the lane, and a *turning* movement has to filter through the opposing movement; i.e. the permitted turning phase.

We propose that a few *through* vehicles can pass the stop line until a *turning* vehicle arrives at the stop line of a shared lane. Once a *turning* vehicle is at stop line, we propose that the flow of *through* and *turning* vehicles from a shared lane will be zero when the opposing flow is greater than the threshold flow. The threshold value for flow is equal to a reciprocal of an acceptable critical gap in opposing traffic. Once the opposing flow is less than or equal to the given threshold value, the *through* and *turning* flows are allowed to flow out from a shared lane using an adjusted flow rate for the *turning* movement. The following steps and equations are used to calculate the stop-line flow for a shared lane:

1. Assume that the signal turns green at *t*. Set the threshold value for the opposing *through* flow equal to $1/a$ where a is an acceptable critical gap in opposing traffic.
2. Check if the opposing *through* flow at time step *t* is less than threshold flow.
   i. If yes, outflow from stop line cell of a shared lane is calculated as follows:
      First, calculate the saturation flow rate for a permitted turn using Equation 23, which is proposed by Akcelik (1989).

$$S_u(t) = \frac{\lambda \theta e^{-\lambda(a-\Delta)}}{1 - e^{-b\lambda}} \tag{23a}$$

$$\lambda = \sum_{l=1}^{N} \frac{\varphi_l q_l}{1 - \Delta q_l} \tag{23b}$$

$$\theta = \prod (1 - \Delta q_i) \tag{23c}$$

In equation 23*a*:
- $S_u(t)$ is the saturation flow rate for a permitted turn in vehicles/second that is subjected to the maximum value of $3600/b$ when the opposing flow is zero where;
- b is the minimum departure headway in second;
- a (in seconds) is the accepted critical gap in the opposing traffic that is safe for *turning* vehicles. It is dependent on human factors and site conditions (such as terrain, speed limits, etc.). It should be calibrated from the field observations.
- Δ (in seconds) is the minimum headway observed in an opposing traffic lane.

Parameters λ and θ are calculated respectively using Equations 23*b* and 23*c*. Summations and multiplications in these equations are for the lanes $l = 1 \ to \ N$ of opposing traffic. φ_l is a bunching factor and q_l is an opposing flow in a lth opposing

traffic lane. For a detailed explanation of Equations 23*a,* 23*b* and 23*c,* refer to Akcelik (1989).

The next step is to calculate the outflow of *through* and *turning* movements (refer to Equations 24 and 25) from the stop-line cell of a shared lane that will be summed up to calculate the total outflow from the stop-line cell of a shared lane (refer to Equation 26).

$$y_{dR}(t) = \min\left(n_{SL}(t) * \gamma_R^t, Q_{sat} * \gamma_R^t, S_u(t) * dt, R_{dR}^t\right) \tag{24}$$

$$y_{dT}(t) = \min\left(n_{SL}(t) * \gamma_T^t, Q_{sat} * \gamma_T^t, R_{dT}^t\right) \tag{25}$$

$$y_{dtotal}(t) = y_{dR}(t) + y_{dT}(t) \tag{26}$$

    ii.   If no, the outflow of the *right turning* movement will be zero. Calculate the demand of the *through* movement that can pass the stop line before a turning vehicle arrives at the stop line using Equations 17 and 18; calculate the outflow of the *through* movement from a shared lane using Equation 21. Also, update the demand of the *through* movement for the next time step using Equation 22.

  3. *t = t+1* and go to step 2.

3.4 The ACTM for balancing lane utilisation

Researchers have used the movement-by-movement approach to model arterial traffic in the CTM that assumes equal utilisation of lanes serving the same movements. Conversely, at signalised intersections, an unequal use of lanes serving the same movements is expected due to the presence of short lanes or shared lanes (Akçelik, 1997). In such cases, to avoid the longer queue, drivers tend to change lanes from high-occupancy lanes to low-occupancy lanes. This behaviour is also confirmed by Sun and Elefteriadou (2012) in their focus group survey and instrumented vehicle-based experiment.

To incorporate such behaviour, this study presents an extension of the lane-by-lane CTM to model lane changes from high to low occupancy lanes. For ease of explaining the proposed balancing technique, refer to the example presented in Figure 8. It shows the arrangement of cells on an arterial link having two *through* lanes and one *right turning* short lane. Each cell number is followed by a lane number; e.g. cell *1(l′)* represents the first cell in lane *l′* from the upstream end of the link. Say the *through* lane *l* has a higher occupancy compared to the *through* lane *l′* due to the presence of the short lane adjacent to lane *l*. In this case, vehicles will shift from lane *l* to *l′*, as shown by dotted arrows. As illustrated, there will be two inflows, namely a *through* flow and a lane change flow in the cells of lane *l′*. Such discretionary lane changes are generally restricted within a channelised zone. We give absolute priority to *through* traffic in lane *l′* and assume that the lane change demand will not be satisfied unless *through* demand on the lane *l′* is completely satisfied during a given time interval. This assumption is also used in one of the lane change algorithms for the CTM developed by Carey et al. (2015).
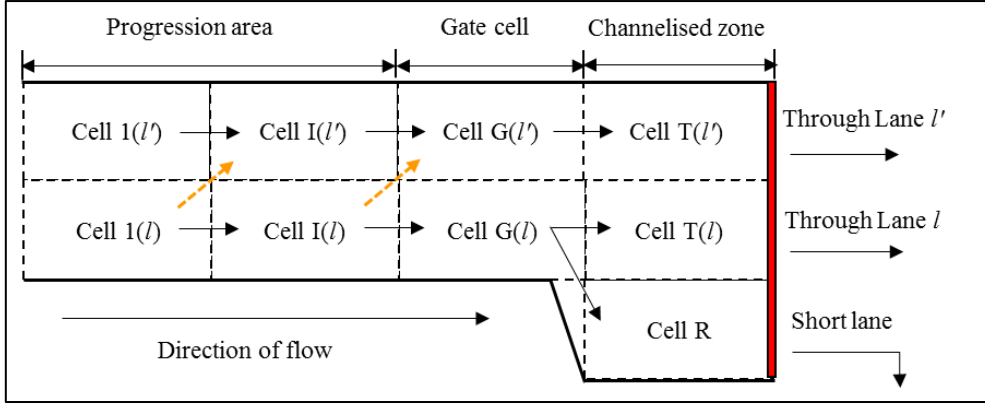
Figure 8: The CTM set up for lane utilisation balancing

The aforementioned example leads to an obvious question: *How many vehicles will shift lanes from lane l to l' and at which location (cell)?* Laval and Daganzo (2006) identified the difference in speed of the two lanes as one of the major motivations of lane changing and proposed a formula to calculate the lane-changing fraction based on the difference in speed of the two freeway lanes. However, for arterials, traffic flow is interrupted by signals with not much significant difference in the speed between the two lanes.

Hence, we propose to model the lane-changing fraction on arterial lanes that serve the same movement as a function of the difference in the queue (occupancy) of the lanes, with the objective to balance the lane utilisation of the two lanes. This might not always be true in practice for the two lanes serving the same movements. For instance, lane *l'* shown in Figure 8 can be shared with left *turning* movements. In such cases, the potential flow shifting from the lane *l* to *l'* can be different. The tendency to change lanes is highly dependent on the driver's behaviour and route choice, which may vary from location to location and should be accounted for. We introduce a calibration factor β to account for such tendency and this is presented in Equation 27. Here, for a given time interval, if $(i+1)^{th}$ cell of *through* lane *l* has a density greater than the critical density, the lane change fraction ($LC_i^{l\ l'}$) for i^{th} cell of *through* lane *l* is calculated based on the difference in the density of $(i+1)^{th}$ cell of *through* lanes *l* and *l'* as follows:

$$LC_i^{l\ l'}(t) = max\left\{0, \beta\left(\frac{n_{i+1}^l(t) - n_{i+1}^{l'}(t)}{N_{i+1}}\right)\right\} \quad (27)$$

Where *l'= l+1 or l'= l-1 and* $\beta \geq 0$. Depending on field observations, the value of β will vary between 0 (no lane changes) to 1(lane-change demand to the maximum value possible). For instance, it is possible that due to their choice of the destination, vehicles do not change lanes even when the queue in the current lane is longer than the adjacent lane. In such cases, β will be set to zero. We suggest that the default value of β should be set as 1 to allow for lane balancing in case of unequal lane utilisation.

The consideration of the aforementioned lane-changing fraction in the CTM can be explained with the help of an example: refer to Figure 8. First, calculate the *through* flow from cell *i* to *i+1* of lane *l'*. If there is still an unused receiving capacity in cell *i+1* of lane *l'* at a time *t*, then it can be filled by a lane-change demand. For this, a lane-change demand is calculated in cell *i* by multiplying the LC fraction and demand in cell *i* of lane *l*. Finally, the flow from cell *i* to *i+1* of lane *l* is calculated taking into consideration the traffic that has already changed lanes.

The algorithm for the abovementioned process is outlined below: for balancing lane utilisation, vehicles change lanes from *l* to *l'* because the queue in lane *l* is expected to be longer than in *l'*. Note *l'* and *l* are adjacent to each other; i.e., *l'= l+1 or l'= l-1*.

Algorithm:

1. *Start, t= 1, Here, $R_R^t = R_{T(l)}^t = N+1$ and $R_{G(l)}^t = N-1$ for an empty cell instead of N.*
2. *Calculate through flow among cells of lane l', $y_{i(l')\to i+1(l')}(t)$ as per Equation 7.*
3. *Initialise $y_{i(l)\to i+1(l')}^{LC}(t) = 0$*
4. *If $R_{i+1(l')}^t - y_{i(l')\to i+1(l')}(t) \le 0$ then go to Step 7.*
5. *Calculate the lane-changing fraction from lane l to l' ($LC_i^{ll'}$) using Equation 27 for all cells in the progression area of lane l. Lane-change demand can be calculated using the following equation:*

$$D_{i(l)\to i+1(l')}^{LC} = LC_i^{ll'} \times \gamma_T^t \times n_i(t) \qquad (28)$$

   This is valid only for cells in the progression area.
6. *If $D_{i(l)\to i+1(l')}^{LC} > 0$, calculate lane-change flow as,*

$$y_{i(l)\to i+1(l')}^{LC}(t) = min\left\{ D_{i,l\to i+1(l')}^{LC}, R_{i+1(l')}^t - y_{i(l')\to i+1(l')}(t), Q(t) \right\} \qquad (29)$$

7. *Except for the outflow of 'G(l)', i.e. the flow into 'R' &'T(l)', calculate the through flow among cells of lane l, as below:*

$$y_{i(l)\to i+1(l)}(t) = min\left\{ n_{i(l)}(t) - y_{i(l)\to i+1(l')}^{LC}(t), R_{i+1(l)}^t, Q(t) \right\} \qquad (30)$$

8. *To calculate the outflow from 'G(l)', i.e. inflow of 'R' &'T(l)', use Equations 11 to 15.*
9. *Hence, the total flow into cell i+1 of lane l' from the upstream cell i of lane l and l' in time step t will be $y_{i(l')\to i+1(l')}(t) + y_{i(l)\to i+1(l')}^{LC}(t)$*
10. *Update the cell occupancies using Equation 4 for time 't+1'.*
11. *t=t+1*
12. *Check if t = the end of the simulation, if no, then go to Step 2. Otherwise, end.*

Note: The above algorithm is limited to lane utilisation balancing for two lanes only. The algorithm can be extended for multiple lanes by:

- Incorporating effects of destination lane at a downstream intersection on lane selection at an intersection; and
- Formulating a multinomial logit model where the utility of each lane will be evaluated in terms of queue length present on it for choosing the target lane from multiple lanes; a similar notion is proposed by Sun and Elefteriadou (2012) as they used queue length as one of the explanatory variables in the utility of the target lanes to capture speed gain advantage.

The above extensions are outside the scope of this paper.

The proposed extensions of the CTM described in Sections 3.2, 3.3 and 3.4 can be used with or without the modification explained in Section 3.1.

4 Discussion on calibration of CTM and ACTM

In this section we discuss the calibration procedure for CTM and ACTM used in this research.

For CTM, the fundamental diagram parameters need to be calibrated. Assuming triangular fundamental diagram the parameters to be calibrated include a) free flow speed (v_f); b) maximum flow rate (saturation flow rate, Q_{sat}); and c) the jam density of queued vehicles (k_j). Other parameters such as critical density ($k_c = Q_{sat}/v_f$) and shockwave speed ($w = Q_{sat}/(k_j - k_c)$) can be estimated once the above three are known.

For the current application, we assume that the free flow speed, v_f is equal to speed limit set for the road. For remaining calibration parameters, sum of the squared error in the back of the queue (BOQ) is used as the objective function. Few of the previous researchers e.g. Srivastava et al. (2015) use error in throughput as an objective function. We tested both the objective functions and found that the values of calibration parameters do not vary significantly. Hence, the objective function used in this research is:

$$\underset{X}{\text{minimise}} \sum_{cycle=1}^{C} \left(BOQ_{cycle} - \widehat{BOQ}_{cycle} \right)^2$$

Where, $X = \left\{ Q_{sat}, k_j \right\}$ (31)

Subject to: $X_L \leq X \leq X_H$

Where BOQ_{cycle}, $\widehat{BOQ}_{cycle}$ are respectively, observed and estimated back of the queue per cycle; $X = $ a set of calibration parameters subject to lower bound, X_L and upper bound, X_H. Genetic Algorithm, which is widely used for calibrating traffic flow models, is coded in MATLAB to find the solution of the non-linear optimisation problem formulated in this study.

The abovementioned process is used for calibration of the ACTM as well. In addition to the triangular fundamental diagram parameters, the ACTM has additional parameters i.e. δ, β, minimum departure headway (a), accepted critical gap in the opposing traffic (b), minimum headway observed in an opposing traffic lane (Δ) and bunching factor (φ_l). These parameters can be added to a set of calibration parameters to get their calibrated values. However, for the experiments presented in section 5 and 6, the aforementioned parameters are obtained as follows:

- Value of δ is calculated using equation 6
- Observed values of a, b,Δ are used and no bunching is assumed i.e. $\varphi_l = 1$ for shared lane modelling experiments presented in section 4.4 and section 5.3.3
- The default value of β (i.e. β=1) is used for lane balancing experiment presented in section 4.5.

5 Numerical experiments and results

5.1 Experiment design

In this section, we progressively evaluate the performance of the proposed ACTM using synthetic data generated from Aimsun-micro which is widely used for research and development applications (Casas et al., 2010). We use simulation because it provides a controlled environment where different traffic conditions can be thoroughly tested with complete knowledge of the traffic states (which is difficult to obtain from the real data). Having said that, the simulation experiments should be carefully designed so that the results are not biased.

Aimsun-micro simulation parameters can have an impact on the CTM and ACTM parameters. For instance, 'speed acceptance' parameter in Aimsun specifies the degree of acceptance of speed limits and it will affect the free flow speed of the traffic stream which can be calibrated for CTM and ACTM. Similarly, value of the 'clearance' parameter in Aimsun determines the distance maintained by a vehicle between itself and the preceding vehicle when stopped. The value of 'clearance' will affect the jam density value (higher the value of clearance, lower will be jam density). It will be taken care of by calibrating jam density for CTM and ACTM. Furthermore, 'Reaction time at stop' needs to be specified

in Aimsun which is a time taken by the first vehicle stopped at a traffic light to react to the traffic light changing to green. The value of 'Reaction time at stop' can affect saturation flow rate and speed of shockwave. Higher the reaction time at stop, lower will be saturation flow rate and shockwave speed. This should be captured through calibration of saturation flow and shockwave speed. In similar manner, we have performed descriptive analysis on the relationship between other Aimsun-micro simulation parameters and the CTM and ACTM parameters. Further, without loss of generality, we use the default parameter values presented in Aimsun for the current experiments. The respective CTM and ACTM parameters are calibrated using the Aimsun-micro simulation data.

Hereafter, the synthetic data and the corresponding traffic states from the Aimsun-micro simulation are termed: 'ground truth'. The data includes individual vehicle trajectories that are processed to estimate: a) the initial boundary conditions for the modelling; and b) the observed measure of performance indicators, such as the maximum at the back of the queue (BOQ). The BOQ is defined as the position of the last vehicle in a queue from the stop line. A vehicle is assumed to be in a queue if its speed is below a threshold speed. For the current application, we have considered this threshold as zero; i.e. the BOQ vehicle has completely stopped.

For the CTM and ACTM simulation:

a) The simulation time interval is 3 seconds[2]. This is fixed for all further CTM modelling performed in Section 4;

b) The cells are numbered starting from the upstream end, and lanes are numbered from the kerb side; and

c) For a fair comparison, the common calibration parameters between these models (such as free-flow speed, jam density, capacity) are kept the same.

The performance of these models is defined in terms of 'Mean Absolute Error' (MAE), i.e. the mean of the absolute difference in the BOQ per cycle, estimated from the model and ground truth.

5.2 ACTM: Modification in queue discharge process

5.2.1 Experiment setup

The experiment is set up for an arterial link consisting of two *through* lanes as illustrated in Figure 9(a), with fixed signals at the intersection. The fundamental diagram and corresponding parameters are presented in Figure 9(b). The free-flow speed (V_f) is 60 km/hr; jam density is 200 veh/km; backward shockwave speed is 12 km/h, and critical density is 33 veh/km.

For the CTM, each lane is divided into cells 50 metres in length ($V_f \times t = 50$ metres). The resulting arrangement of cells is shown in Figure 9(a). The ground truth is generated for the following two cases:

• *Case-1: Under-saturated traffic condition*: The demand is less than the capacity of the signalised intersection, and the queue is expected to clear at the end of the green phase; and

• *Case-2: Over-saturated traffic condition*: The demand is more than the capacity, and the queue is expected to grow with time.

Performance of the following models are compared:

• Traditional CTM (CTM)

• ACTM with start-up loss (ACTM-1a)

• ACTM with shockwave effect (ACTM-1b)

• ACTM with start-up loss and shockwave effect (ACTM-1a,b)

---

[2] Further reducing the time step will provide an opportunity to reduce the cell length, which in turn should increase the BOQ estimation accuracy from the traditional CTM. However, it will increase the computation efforts. There is a trade-off between the computation efforts and accuracy.

- CTM modified by Srivastava et al. (2015) to consider start-up loss (Sri-CTM): the common calibration parameters; i.e. the fundamental diagram for the Sri-CTM is the same as that used for the CTM and ACTM. The additional parameter (jam demand) is calibrated as described by Srivastava et al. (2015).


(a)

(b)
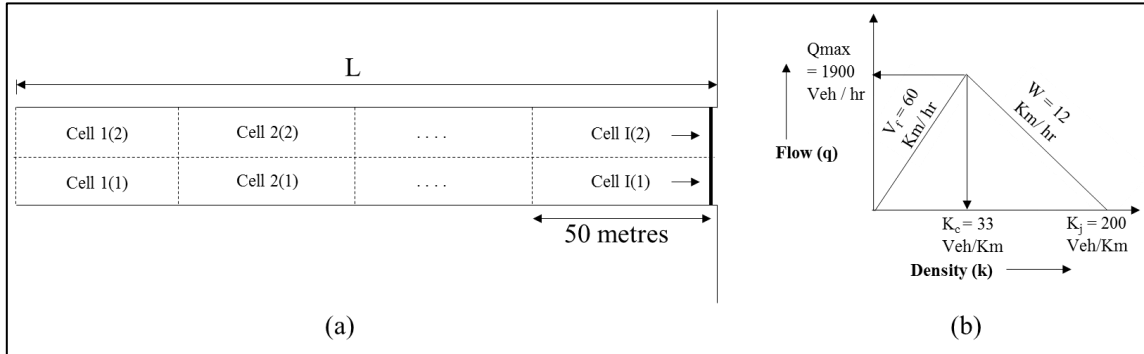
Figure 9: Experiment details for the queue discharge process modification in ACTM

5.2.2   Experiment results

The BOQ from 60 signal cycles (averaged over lanes 1 and 2) for Case-1 and Case-2 are presented in Figure 10 and Figure 11, respectively. In Figure 10 and Figure 11(a) the x-axis is the signal cycle in the order of time, and the y-axis is the BOQ in metres, estimated during the corresponding signal cycle. Note: The y-axis scale for the two Figures is different; this is to better illustrate the differences between the models. A solid line, a line with dot markers, a dotted line with a square, a line with a cross, a line with dashes, and a line with a triangle, represent results from the ground truth, CTM, ACTM-1a, ACTM-1b, ACTM-1a,b and Sri-CTM, respectively. For all experiments henceforth, the results are presented from the second signal cycle because the first cycle is considered as the warm-up period for the simulation.
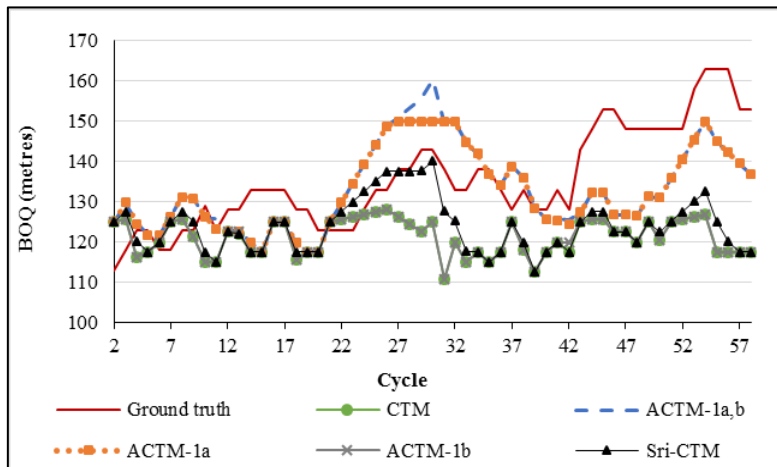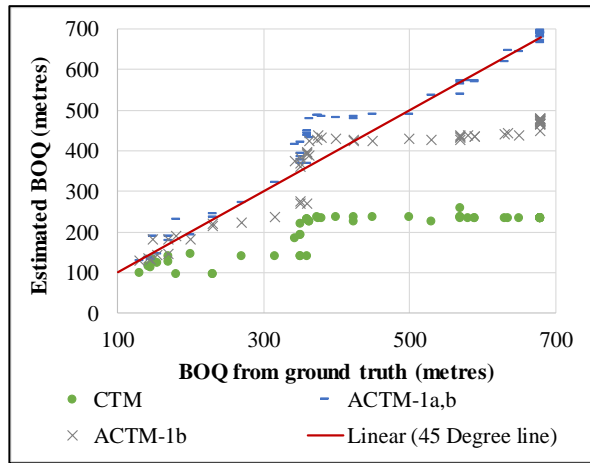

Figure 10: BOQ comparison considering a modification in the queue-discharge process in the ACTM (refer to Section 3.1) for Case-1: Under-saturated traffic condition
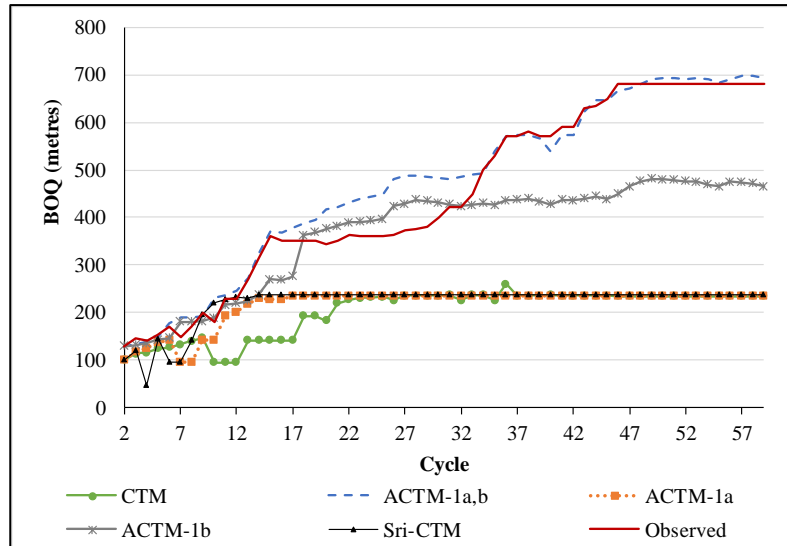
(a)
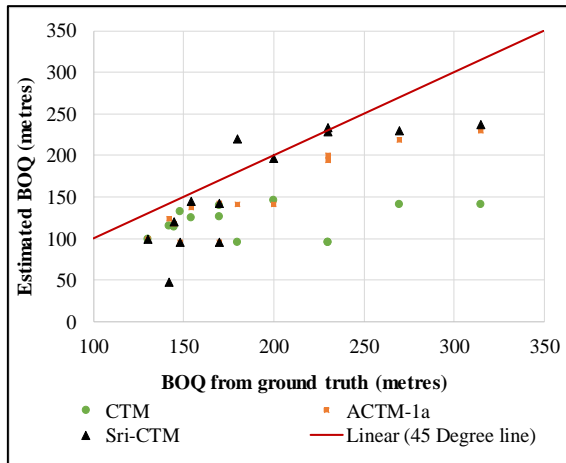
(b)   (c)

Figure 11: BOQ comparison considering modification in the queue-discharge process in the ACTM (refer to Section 3.1) for Case-2: Over-saturated traffic condition: a) time series of BOQ over different cycles; b) Estimated versus ground truth of BOQ for the first twelve (mostly under-saturated) cycles; c) Estimated versus ground truth BOQ for all the cycles.

Discussion for Case-1: Under-saturated traffic (see Figure 10)

- The MAE for the ACTM-1a, Sri-CTM and CTM is 10m, 14m and 16 m, respectively. Both the ACTM-1a and Sri-CTM consider start-up loss and consideration of which improves the BOQ estimation. The results indicate that the ACTM-1a produces smaller errors compared with the Sri-CTM. BOQ values estimated by the ACTM-1a and Sri-CTM are significantly different (at 95% confidence level).

- Figure 10 illustrates that the CTM, in general, underestimates the BOQ. Whereas, the ACTM-1a estimates the BOQ closer to the ground truth.

- For under-saturated traffic conditions, the queue developed during the red phase is cleared during the green phase of the next cycle. The arrival flow during the green phase is generally low and hence consideration of the shockwave effect only (ACTM-1b) does not contribute to any improvement. The two plots in Figure 10 for the CTM and ACTM-1b overlap with the MAE of 16m each. Similarly, the plots for the ACTM-1a,b and ACTM-1a overlap.

From the above analysis it can be conclude that during under-saturated traffic conditions, the consideration of start-up loss improves the BOQ estimation accuracy, and consideration of the shockwave effect is redundant.

Discussion for Case-2: Over-saturated traffic (*see* Figure 11)*:*

- Refer to Figure 11(a). The queue starts building up during the first twelve cycles. Thereafter, the system is saturated with the queue overflowing over different cycles.
- Similar to Case-1 during the initial twelve cycles, the consideration of start-up shows significant improvement. Refer to the Figure 11(b) where the x-axis represents the values of the BOQ from ground truth, while the y-axis represents the BOQ values estimated by the ACTM-1a (squares), Mod-CTM (triangles) and CTM (dots) for the initial twelve cycles. The ACTM-1a and Sri-CTM are closer to ground truth than the CTM. The MAE during these cycles for the ACTM-1a, Sri-CTM and CTM is 36m, 33m and 56m, respectively. A t-test between the CTM and ACTM-1a indicates that the difference in their errors is statistically significant at 95% confidence level. However, the t-test between the ACTM-1a and Sri-CTM indicates that the difference in error is not statistically significant at 95% confidence level.
- The MAE, considering all 60 cycles, is 185m, 167m, 163m, 64m and 37m for the CTM, ACTM-1a, Sri-CTM, ACTM-1b and ACTM-1a,b, respectively.
- The consideration of backward shockwave plays a significant role after the twelfth cycle where the queue starts overflowing into the next cycle. Graphs in Figure 11(c) presents the ground truth (x-axis) and estimates (y-axis) of the BOQ using the CTM(dots), ACTM-1b (cross) and ACTM-1a,b (dash) for all 60 cycles. The BOQ estimated by the ACTM-1b and ACTM-1a,b are closer to the ground truth than the CTM. Here, the ACTM-1a,b has a better performance than the ACTM-1b. This is because the ACTM-1b does not consider the start-up loss, the error for which can accumulate over time.

From the above analysis it can be concluded that during over-saturated conditions, the consideration of a start-up loss and shockwave effect significantly improves the BOQ estimation accuracy.
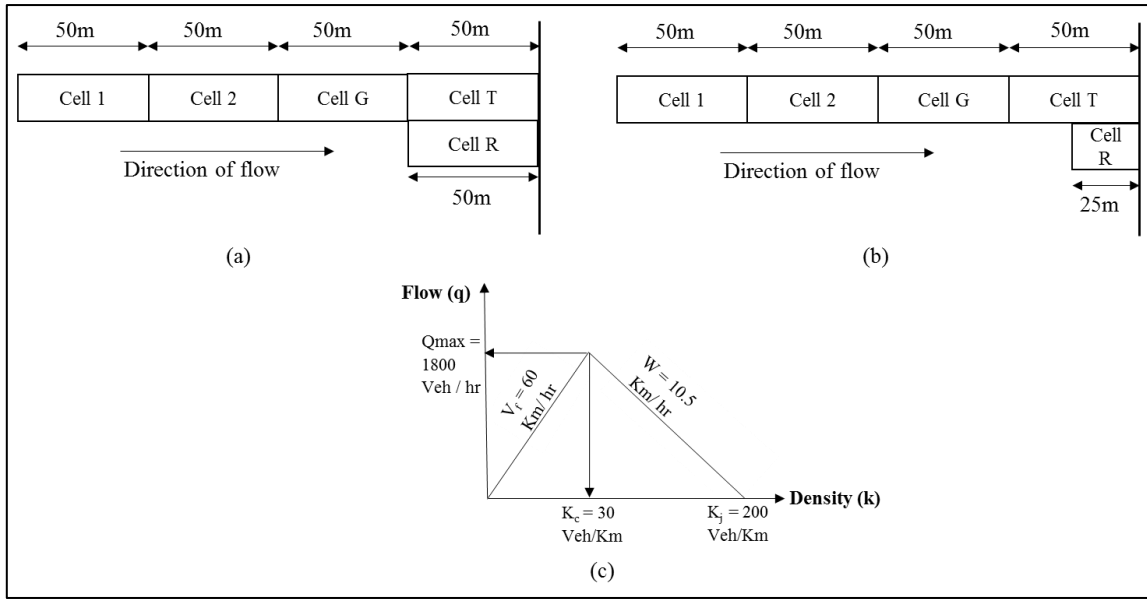
5.3 The ACTM for Short-Lane blockages and spillbacks

5.3.1 Experiment setup

To test the ACTM for modelling short-lane blockages and spillbacks, the following lane configurations are tested:

- *Case-1:* an arterial link with *through* movement and a short right turn lane of length equal to single cell length. The cell arrangement is shown in Figure 12(a) where a short lane– 50 metres in length–consists of a single cell named R.
- *Case-2:* an arterial link with *through* movement and a short right turn lane of length less than single cell length. The cell arrangement is shown in Figure 12(b) where a short lane–25 metres in length–consists of a single cell named R, which is smaller than other cells.

The fundamental diagram for a link in both cases is shown in Figure 12(c). *Through* and *turning* movements simultaneously receive the green time. We assume that the average turning proportions in cell G are known for the CTM simulation.

Figure 12: Experiment details for testing short-lane blockages and spillback extensions in the ACTM (refer to Section 3.2)

The BOQ estimated by following models are compared using the MAE:
- CTM: Traditional CTM
- ACTM-1: ACTM with start-up loss and shockwave effect only
- ACTM-1&2: ACTM with start-up loss, shockwave effect and short lane extension
- Liu-CTM: CTM based short lane model proposed by Liu and Chang (2011)

5.3.2 Experiment results

Figure 13(a) and Figure 13(b) show the BOQ in the *through* lane plotted against the signal cycle for 10 cycles for Case – 1 and Case – 2, respectively. A solid line, a line with dots, a line with dashes, and a line with a triangle represent results from ground truth, the CTM, ACTM-1, ACTM-1&2 and Liu-CTM, respectively.

Discussion for Case-1: The length of cells in the short lane is consistent with the other cell lengths - refer to Figure 13(a):
- Here, the MAE in the BOQ estimation is 11m, 10m, 9m and 11m for the CTM, ACTM-1, ACTM-2 and Liu-CTM, respectively.
- Though the performance of the ACTM-1 varies compared to the CTM due to the inclusion of the start-up loss, it does not show any significant improvement in estimating the BOQ over the CTM. In the current experiment, the simulation is performed for under-saturated traffic with a low-arrival flow during the queue discharge.
- Performance of the Liu-CTM matches with that of the CTM. This is because to model the flow in the short turning lane, it uses a similar approach as the CTM diversion operation.
- The BOQ estimated by the ACTM-1&2 overlaps with that of the ACTM-1. This is because a maximum of 10 vehicles (jam density being 200 veh/km) can be accommodated in each cell and there will be a spillback from the short turning lane when the eleventh turning vehicle arrives at the entrance of a short lane. As the difference between N and N+1 is small, the occupancy of cell T does not vary significantly as the occupancy of cell R increases from N to N+1. Hence, the short lane extension proposed in this study is not needed when the short lane length is equal to the cell length selected.

Discussion for Case-2: The length of a cell in the short lane is shorter than other cell lengths - refer to Figure 13(b):

- Here, the MAE for the BOQ estimation is 25m, 25m, 7m and 24m for the CTM, ACTM-1, ACTM-1&2 and Liu-CTM, respectively.
- The CTM overestimates the BOQ because in the CTM, once cell R reaches capacity, flow in cell T is stopped. This leads to vehicles queuing on the upstream of cell T and an empty space is created in cell T.
- The BOQ estimated by the ACTM-1 overlaps with the CTM. This is similar to Case-1 because the demand for these two cases is the same.
- The BOQ estimated by the Liu-CTM is close to the CTM but shorter by a length of a vehicle because, as per Liu and Chang (2011)'s model, once cell R reaches capacity, flow into cell T is not stopped but is reduced (to *through* vehicles in the upstream cell G multiplied by the proportion of *through* vehicles in cell G); however, the flow of the turning vehicles is stopped. In reality, both *through* and *turning* vehicles can flow into cell T. Hence, the Liu-CTM also overestimates the BOQ.
- The ACTM-1&2 estimates the BOQ closer to ground truth as it can model the common space shared by the *through* and *turning* vehicles in cell T closer to reality. An estimation error of the ACTM-1&2 is approximately 3.5 times lower than the traditional CTM, which is statistically significant at 95% confidence level.

From the above analysis, it can be concluded that the proposed modifications (Section 3.2) for the short lane improves the BOQ estimation accuracy of the CTM when the length of one of the cells in the short lane is shorter than the length of normal cells.
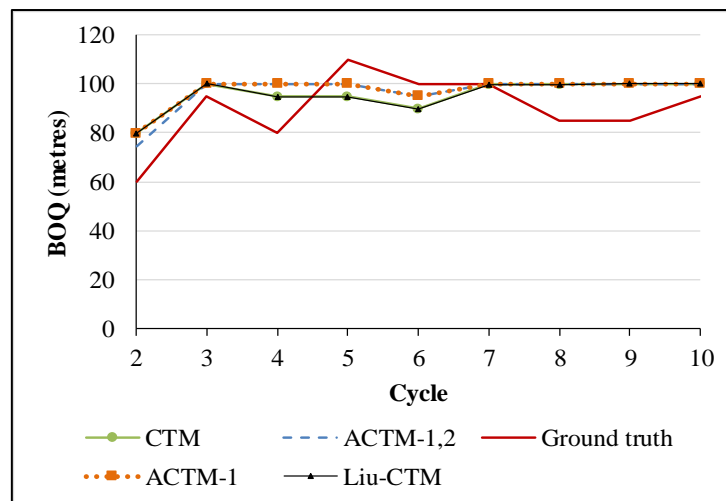
(a) Case – 1**:** short lane length is equal to the cell length
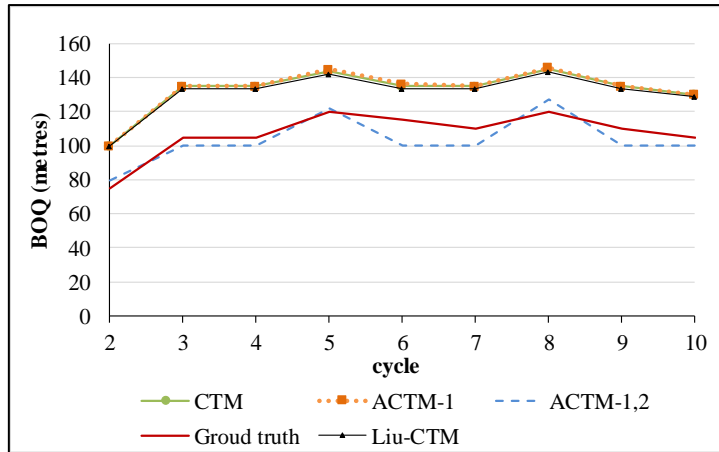
(b) Case – 2**:** short lane length less than cell length

Figure 13: BOQ comparison for short lane blockages and spillback extensions in the ACTM (refer to Section 3.2)

5.4 The ACTM for Shared Lane modelling

5.4.1 Experiment setup

To test the proposed extension for modelling a shared lane using the ACTM (refer to Section 3.3), a T-intersection, illustrated in Figure 7, is simulated. Here, a single lane is shared by a *through* movement and a *permitted right turn,* which is opposed by a *through* movement from the opposite traffic. Each link is divided into cells of equal length as shown by the dotted lines in Figure 7. Both movements simultaneously receive green time where the *right turn* must give way to the opposing *through* traffic.

5.4.2 Experiment results

The BOQ per cycle on a shared lane (Figure 7), obtained from the ACTM with a shared-lane extension only (ACTM-3), and the ACTM with a queue discharge modification and a shared-lane extension (ACTM-1&3), are compared with the corresponding ground truth for an hour of simulation (i.e. 40 signal cycles) and the result is presented in Figure 14. Here, the performance of the ACTM is not compared to the traditional CTM due to the absence of a shared-lane modelling technique in the traditional CTM. We can observe that the BOQ estimates from the ACTM-3 have a similar pattern to ground truth. The MAE is 18 metres, indicating that the model under/over-estimates the BOQ by approximately five vehicles, which is reasonable. Also, the difference in the BOQ estimated by the ACTM-1&3 and ACTM-3 is not statistically significant, indicating that the addition of the start-up loss and shockwave effect does not improve the ACTM further. This is because the queue discharge process from the shared lane is frequently interrupted by opposing vehicles, resulting in a non-continuous discharge process, which is captured by the ACTM-3 only.

26
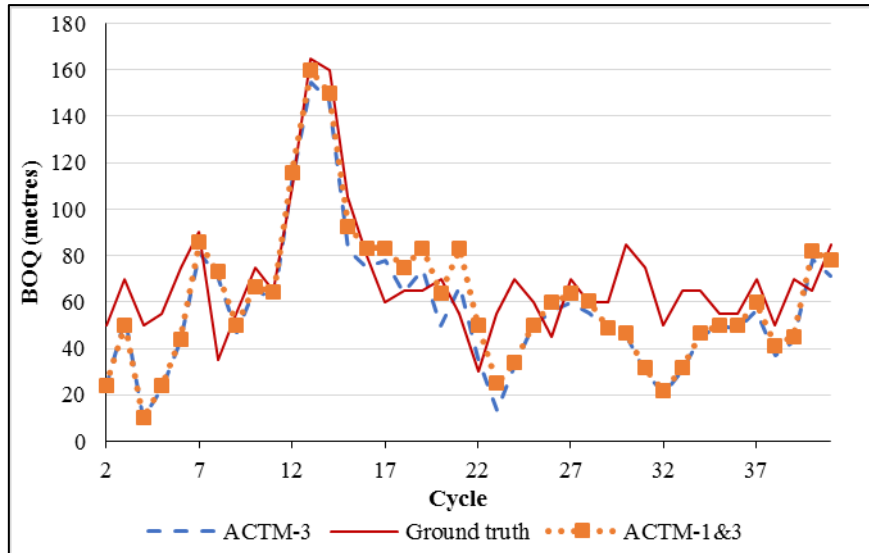
Figure 14: BOQ on a shared lane considering shared lane modifications in the ACTM (refer to Section 3.3)

5.5 The ACTM lane utilisation balancing ability

5.5.1 Experiment setup

The ACTM proposes that a lane utilisation balancing modification should be introduced when the need for the balancing of lanes arises due to the difference in the length of queues on two lanes. The effectiveness of a lane utilisation balancing ability of the ACTM is tested on an arterial link shown in Figure 15, which illustrates the geometry along with the cell arrangement for the current experiment. The fundamental diagram presented in Figure 12(c) is considered for the study link. Here, *through* and *right turning* movements simultaneously receive the green signal.
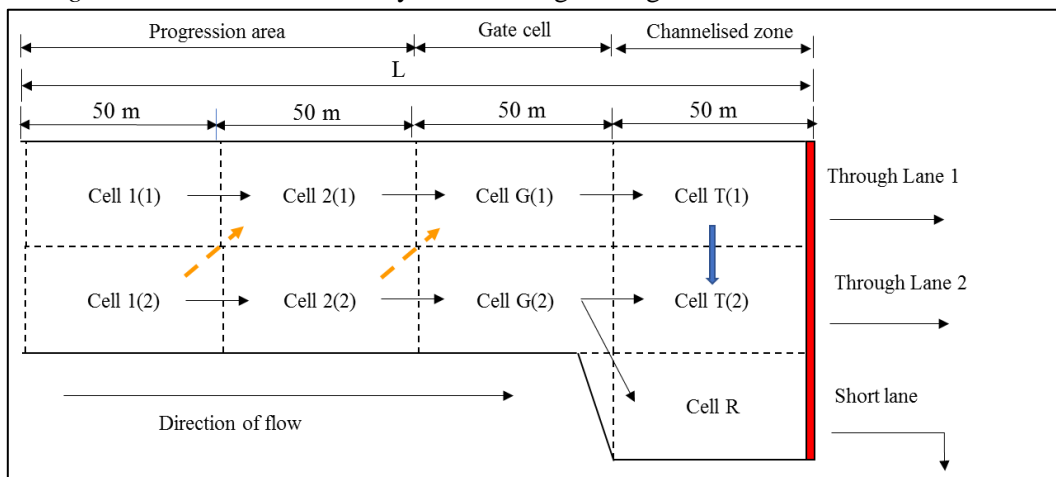
Figure 15: Experiment details for lane utilisation balancing

In Figure 15, lane 1 is only serving the *through* movement whereas lane 2 is serving *through* as well as *right turning* movements until 'cell G(2)'. The queue on the *through* lane 2 is observed to be longer than the queue on the *through* lane 1 due to the spillback from a short turning. In such cases, to avoid long queues the *through* vehicles may change the lane from 2 to 1 (*see* dashed arrows in Figure 15). Furthermore, during the spillback, if 'cell T(2)' is vacant (and the lane changes in the channelised zone is allowed) then the *through* vehicles may change lanes from 'cell T(1)' to 'cell T(2)' (*see* solid bold arrow in Figure 15).

To validate the lane unitisation balancing extension of the ACTM, we compare the BOQ values obtained from the following models:

- CTM: Traditional CTM
- ACTM-1: ACTM with start-up loss and shockwave effect
- ACTM-1&2: ACTM with short lane extension in addition to start-up loss and shockwave effect
- ACTM-1,2&4: ACTM with lane utilisation balancing ability in addition to ACTM-1&2

Here, the extension for shared lanes is not applicable, so it is not considered.

5.5.2 Experiment results

Figure 16 presents plots of the BOQ per cycle for *through* lane 1 and 2. The lane number is shown on the top-left of each plot. A solid line, a line with dots, a dotted line with squares, a line with a cross, and a line with dashes represent results from ground truth, CTM, ACTM-1, ACTM-1&2 and ACTM-1,2&4, respectively. The analysis of plots is presented below:

- The MAE per lane is 52m, 49m, 47m and 20m for the CTM, ACTM-1, ACTM-1&2 and ACTM-1,2&4, respectively.
- A t-test was performed to check if the difference in the errors is significant at 95% confidence. It is observed that the difference in the errors of the BOQ in each lane by the CTM, ACTM-1 and ACTM-1&2 is not statistically significant at 95% confidence, which is also evident in Figure 16. Observed queues clear during a single cycle without overflowing into the next cycle and the arrival flow during a queue discharge is low. Hence, the modification in a queue discharge does not have a significant impact on the performance of the ACTM-1. Similarly, the short lane has a single cell of the same length as other cells and therefore the impact of a short-lane extension is not significant (consistent with the results in Section 5.3.2).
- Figure 16 shows that the observed queue on lane 2 is longer than the queue in lane 1 and the lane utilisation balancing ability of the ACTM-1,2&4 improves the BOQ estimation accuracy compared to that of the CTM. It is observed from the simulation that after the sixth cycle, every cycle has a spillback from the short lane, which creates an empty space in 'cell T(2)' and vehicles change lanes from 'cell T(1)' to 'cell T(2)'. The ACTM-1,2&4 captures this lane change and hence BOQ estimated for lane 1 is closer to ground truth. The ACTM-1,2&4 has a three-times-lower error rate than the CTM and the difference in errors is significant at 95% confidence.
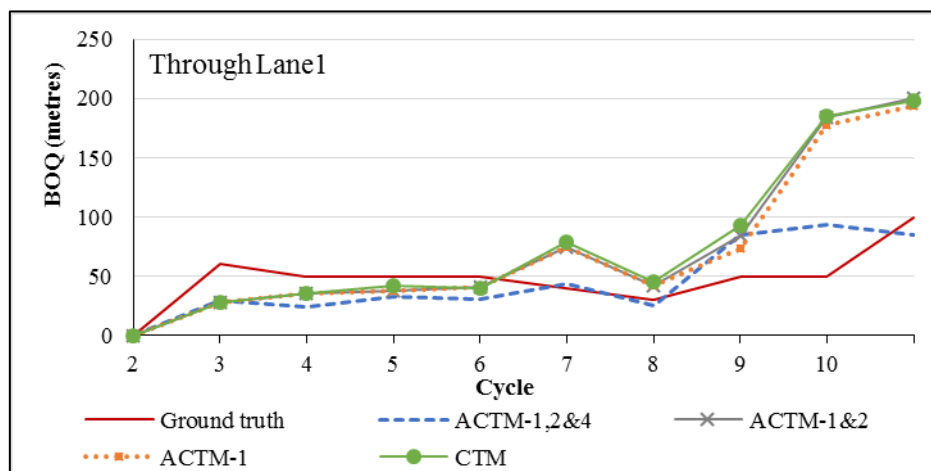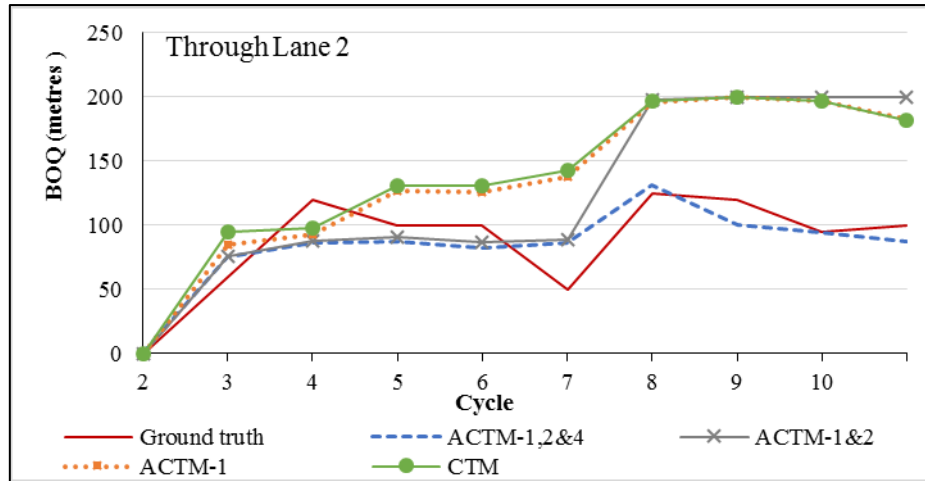
Figure 16: BOQ comparison for an extension in the ACTM to include lane utilisation balancing ability (refer to Section 3.4)

From the above analysis, it can be concluded that the proposed ACTM, with suitable modifications and extensions, can simulate traffic on the arterial link closer to ground truth.

To further test the effectiveness of the ACTM under different traffic demands and cell lengths, the synthetic data for an arterial corridor with four intersections is obtained from Aimsun-micro and different traffic demands are used for simulation. The performance of the proposed ACTM is compared with ground truth observed from synthetic data under different demands. The comparison shows that the ACTM can simulate different demands for different lane configurations closer to reality (average accuracy of 80%), which is in agreement with the results presented in Sections 5.2 to 5.5. The results of this comparison are not presented here due to space constraints. A noteworthy observation from the results is that the proposed modifications (ACTM) did not significantly affect the computational time of the traditional CTM. Both models, the ACTM and the traditional CTM were coded in Matlab and tested on an Intel Core i7-6700 3.4 GHz processor with 16.0 GB RAM. On average, the ACTM and the traditional CTM took 115 and 98 milliseconds, respectively, to simulate a time period of one hour. This is approximately 15% increase in the computation time. Note, it is expected that the increase in the computation time will not be proportional to the size of the network because the aforementioned modifications are needed only for certain sections of the arterial network.
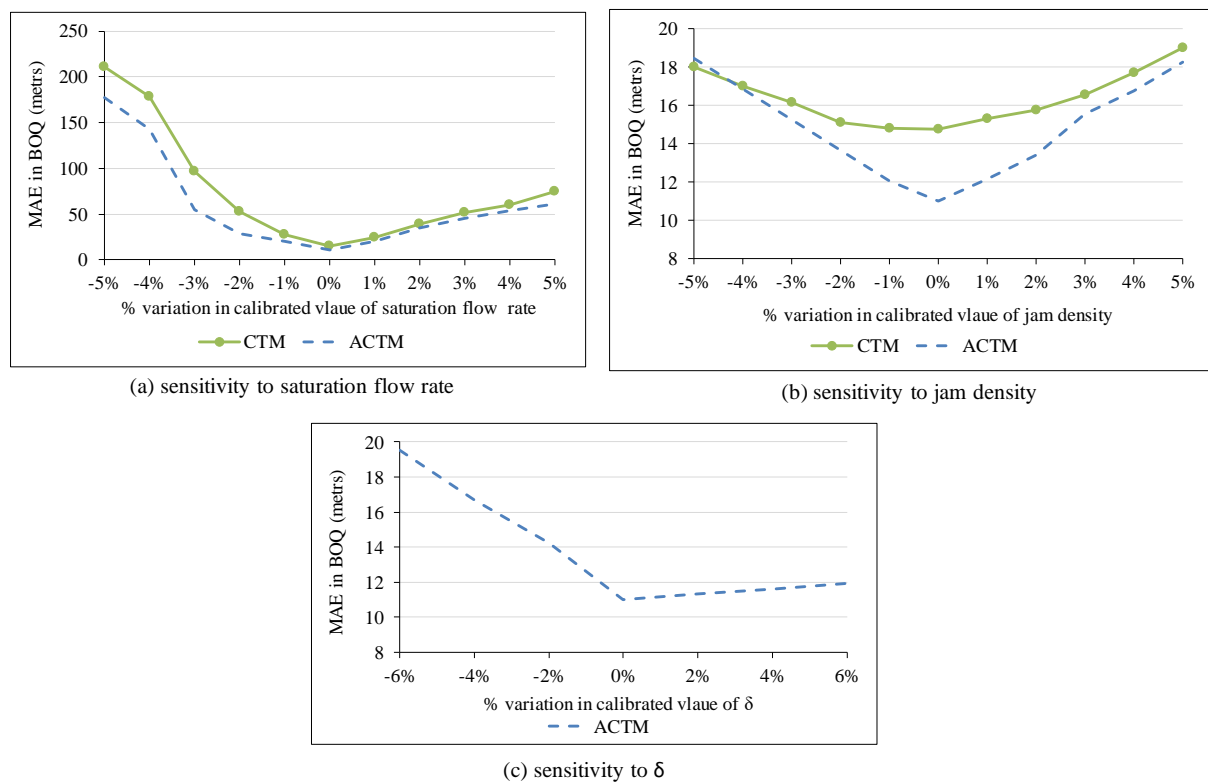
5.6 Sensitivity analysis

To understand how sensitive the modified/traditional model's performance is to the calibration parameters, the sensitivity analysis is performed, and results are presented here. At a selected time step, one of the calibration parameters is varied at a regular interval between lower and upper bounds of the parameter from its calibrated value, keeping all other parameters constant, and the error in BOQ is calculated to evaluate the model's performance.

Firstly, the saturation flow rate is varied and its impact on the CTM's and ACTM's performance is analysed. The saturation flow rate is changed by ± 5% of its calibrated value and the corresponding error in BOQ estimated by CTM and ACTM are presented in Figure 17(a). Noteworthy observations found from sensitivity analysis are; a) when the saturation flow rate is decreased (increased) by 1% to 5% from its calibrated value, the error in BOQ approximately varies from 2 to 14 times (2 to 5 times) compare to the error obtained at the calibrated value. This implies that both models, i.e. CTM and ACTM, are sensitive to saturation flow rate; b) The error in BOQ increases at a higher rate when the value of the saturation flow rate is less than the calibrated value as compared to the error in BOQ

observed when the value of the saturation flow rate is more than the calibrated value; and c) BOQ is overestimated when the value of the saturation flow rate is less than the calibrated value and vice versa.

Furthermore, the jam density parameter is varied similar to the saturation flow rate and the results are presented in Figure 17(b). The errors in BOQ estimated by the CTM and ACTM is respectively, 1.2 times and 1.6 times the error observed at the calibrated value when jam density value is increased or decreased by 5%.

The ACTM has an additional calibration parameter i.e. δ. Its value is changed similarly to the above parameters. The results are presented in Figure 17(c) from which it can be concluded that the error in BOQ is 1.8 times (1.08 times) the error observed at the calibrated value when the calibrated value of δ is decreased (increased) by 5%. Such a lower variation in the error implies that the performance of ACTM is not as sensitive to jam density and δ as saturation flow rate.

(a) sensitivity to saturation flow rate

(b) sensitivity to jam density

(c) sensitivity to δ

Figure 17: Sensitivity analysis for CTM and ACTM

In the following section, the proposed ACTM is applied on real arterial test sites in Brisbane, and its performance is validated against field observed data.

6 Field test

6.1 Data Collection

Data is collected at three sites in Brisbane using video cameras. Details of each site are given below:
- **Site 1:** Southbound Coonan Street between its intersection with Allwood Street at upstream to its intersection with Westminister Road at downstream. A survey was conducted between 16:00 to 17:00 on a working Thursday, 22nd March 2017.

- **Site 2:** Northbound Ipswich Road between its intersection with Villa Street at upstream to its intersection with Aubigny Street at downstream. A survey was conducted between 7:30 to 8:30 and 17:15 to 18:15 on a working Friday, 24th August 2018.
- **Site 3:** Southbound Oxley Road between its intersection with Hughes Lane at upstream to its intersection with Clivenden Ave at downstream. A survey was conducted between 7:30 to 8:30 and 17:15 to 18:15 on a working Tuesday, 21st August 2018.

The following data was extracted from the above links using a video:

- Vehicle count entering each lane every 5 seconds;
- Vehicle count leaving each lane every 5 seconds;
- Signal cycles and phase durations serving the traffic from the arterial link;
- BOQ observed on each lane of the arterial link every 5 seconds;
- Turning proportions; and
- At Site 3, the vehicle count leaving each lane of northbound Oxley Road every 5 seconds.

Interestingly, during the survey period, the traffic contained mostly cars. The proportion of heavy vehicles or special vehicles was negligible.

6.2 Simulation using the CTM

To be consistent with the data extraction, a time interval of 5 seconds is used for the CTM simulation. Sketches of the study links at the three sites, along with cell arrangements (cell lengths and names) for the CTM simulation, and corresponding calibrated fundamental diagrams are presented in Figure 18. The fundamental diagram is observed to be consistent for all lanes on a link.
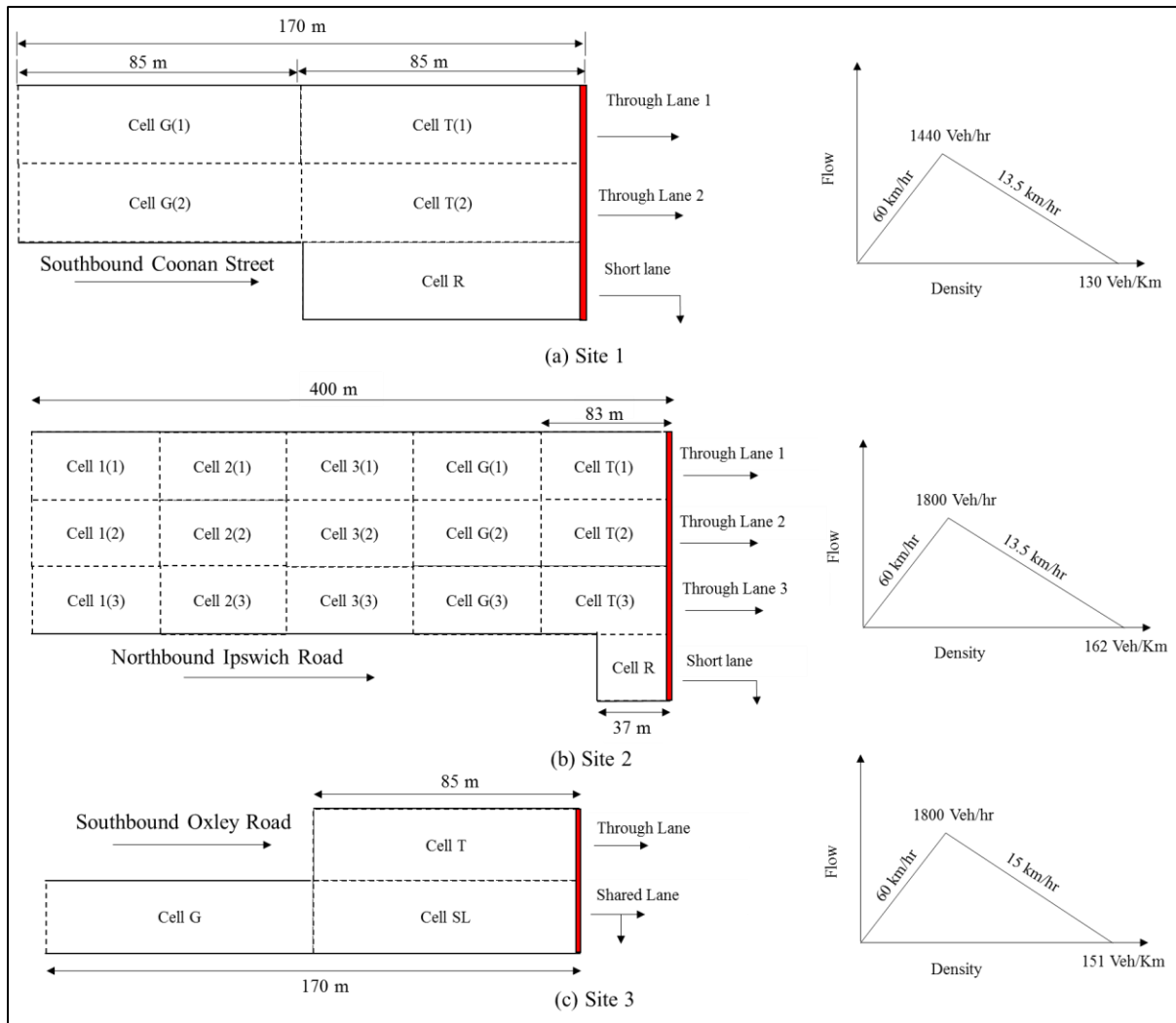
Figure 18: Details of the arterial link studied and the CTM configuration

Depending on the requirement of the link geometry at each site, traffic is simulated using boundary conditions extracted from the extracted real data and suitable extension/s proposed in the ACTM as follows:

a) **Site 1**: During the survey period the *right turning* demand was not significant. There was no spillback from the short lanes. There were no significant differences in the queues on lane 1 and 2, which means the lane utilisation balancing will not make a significant contribution in the ACTM. Also, a shared lane does not exist. The ACTM is used to estimate the BOQ, which is compared with the estimation from the CTM to evaluate the improvement achieved by a modified queue discharge process in the ACTM. Both *through* lanes (lane 1 and 2) were congested for most of the signal cycles during the study period. Incorporating a backward shockwave effect in each cell is expected to improve modelling results.

During most of the cycles, it was observed that the saturation rate dropped to 740 veh/hr during the first 5s of green. Therefore, the value of 'δ' in the ACTM is defined as 0.52. Figure 19(a) illustrates the flow rate profile at the stop line considered during green for the ACTM. The corresponding profile for the traditional CTM is presented in Figure 19(b).
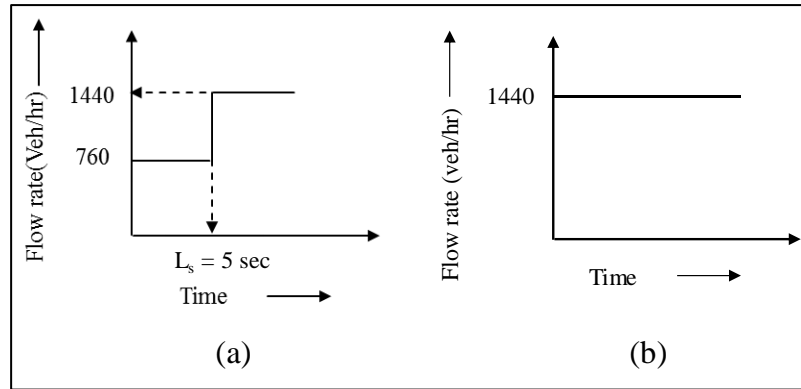
Figure 19: Flow rate profile for the CTM simulation a) ACTM; b) traditional CTM

b) **Site 2:** The short lane spillbacks and blockages were frequently observed during the survey period. Here, the ACTM is used to model the short lane spillbacks and blockages.

c) **Site 3:** The right turners from the shared lane are served by a permitted phase for a few of the cycles during the survey period. Here, the ACTM can model the vehicle interactions on the shared lane during the permitted turning phase.

6.3 Results

The results of the BOQ estimation from the ACTM and CTM for the three sites are presented here. The results are compiled from the simulation configurations of 5 seconds simulation time and cell lengths of 85 m as presented in Figure 18.

6.3.1 Site 1

Figure 20 shows that the ACTM (dashed line) gives BOQ values closer to the observed (solid line) during most of the signal cycles as compared to the traditional CTM (solid line with dot marker). To quantify the improvement in accuracy of the CTM due to the proposed modification, the MAE is calculated. The results are averaged over 32 cycles per lane. The MAE for the ACTM is 23m and 19m for lane 1 and lane 2, respectively. Whereas, for the traditional CTM, the MAE is 48m and 24m for lane 1 and lane 2, respectively. A t-test – performed to check if differences in errors for the ACTM and the CTM are significant – confirmed that the ACTM can significantly improve the accuracy of the CTM application on an arterial network. The ACTM gives an approximately 2 times lower estimation of error compared to the traditional CTM, showing improvement in performance of the CTM after the modification.

(a) Lane 1   (b) Lane 2
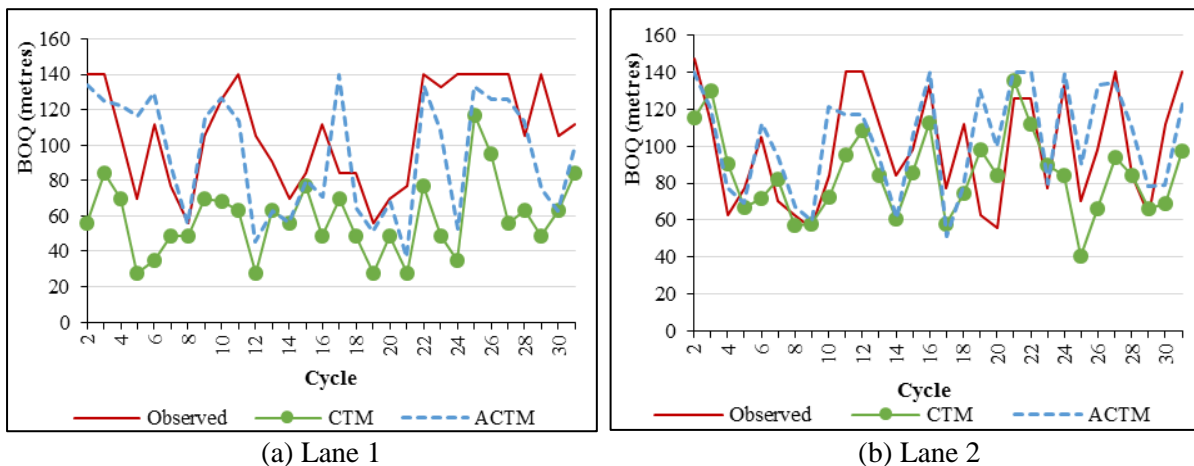
Figure 20: BOQ comparison for Site 1

6.3.2 Site 2

Observed data shows vehicles from the short lane spillback during most of the cycles. Thus, the ACTM is expected to model occupancy of the *through* lane adjacent to the short lane more accurately than the traditional CTM. Figure 21 presents the observed (solid line) BOQ on the *through* lane 3 that is adjacent to the short lane during the time 16:15 to 17:15 (PM peak) as well as corresponding estimates from the ACTM (dashed line) and the traditional CTM (solid line with dot marker). For lane 3, the CTM and the ACTM provide the MAE of 106m and 36m, respectively. Also, the t-test showed that the difference in error between the CTM and the ACTM is significant. Thus, it can be concluded that the ACTM offers a significant improvement for modelling short lane spillbacks and blockages. Similar results were observed for the simulation of traffic from 7:30 to 8:30 (AM peak).
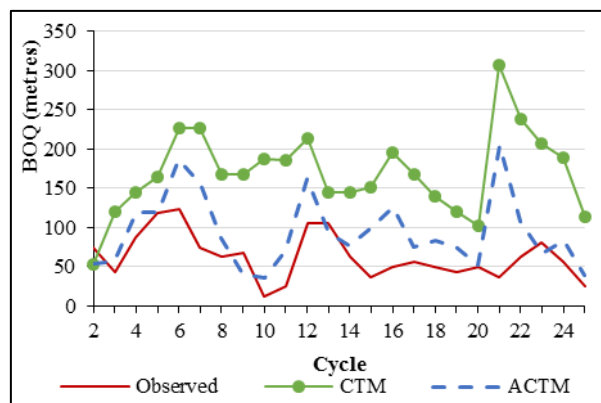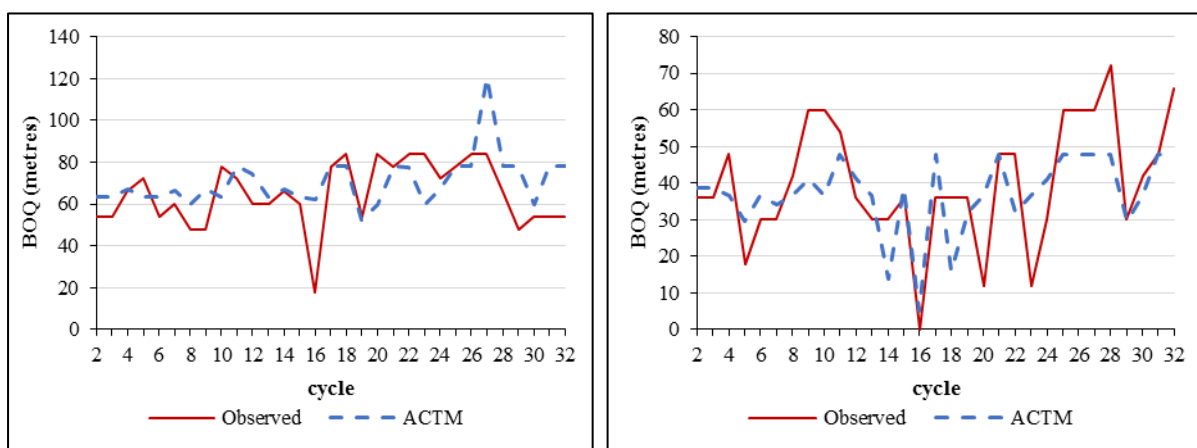

Figure 21: BOQ comparison for Site 2

6.3.3 Site 3

The ACTM is used to model the arterial link at Site 3 that has a shared lane. Figure 22 presents the BOQ from the ACTM (dashed line) and a real observation (solid line) on the shared lane and adjacent exclusive *through* lane from 7:30 to 8:30 (AM peak). The MAE is 12m for the BOQ on the shared lane as well as on the exclusive *through* lane.

Similarly, during the PM peak (17:15 to 18:15) the MAE is 17m and 10m, respectively, for the shared lane and the exclusive *through* lane. As the ACTM under/over-estimates the BOQ by only 1 or 2 vehicles, it can be concluded that the ACTM can satisfactorily model traffic interactions on the shared lane.

(a) Shared lane   (b) Exclusive through lane

Figure 22: BOQ comparison for Site 3

7 Conclusion

The research is aimed to improve the performance and capabilities of the CTM for simulating complex arterial networks. For this, the paper presents an Arterial Cell Transmission Model, named ACTM that models the arterial links to capture:

- *Shockwave:* The formulation of the traditional CTM is modified to incorporate consistent detection and propagation of shockwave by tracing backward shockwave generated during each signal cycle, which significantly affects the accuracy of queue estimation.
- *Short lane:* The interaction of vehicles turning into the short lane with through vehicles in an adjacent lane is modelled by adjusting the capacity allocation of cells. This provides flexibility to model short tuning lanes with cell length shorter than the minimum required cell length for the given simulation time step. This modification enhances the ability of the traditional CTM to effectively model blockages and spillback from a short lane.
- *Permissive turn on shared lane:* A gap acceptance behaviour is incorporated in the traditional CTM to model a shared lane and interaction between its movements when one of the movements on the shared lane must give way to opposing through traffic.
- *Balancing lane utilisation:* The lane utilisation balancing between two lanes is modelled by first comparing the queue length formed on two adjacent lanes serving the same movement and then identifying the unequal lane utilisation. Furthermore, an equation is proposed to calculate a number of vehicles willing to change the lane to avoid the long queue and an algorithm is presented to incorporate such lane changes in the traditional CTM. Such lane utilisation balancing is important for realistic queue length estimation on each lane.

The proposed model has been thoroughly tested using synthetic data and validated using field observed data. The BOQ estimates from the ACTM are closer to observed values compared to the traditional CTM. Testing using synthetic data indicates 18% - 80% improvement. Similarly, test using field data showed 20% - 60% improvement. From the analysis the following conclusions can be made:

a) During over-saturated conditions, the consideration of a start-up loss and shockwave effect significantly improves the BOQ estimation accuracy. During under-saturated traffic conditions, the start-up loss improves the BOQ estimation accuracy, but consideration of the shockwave effect is redundant.

b) If the length of the cells in the short lane is shorter than the normal cell length, then the proposed extension for the short lane significantly improves the BOQ estimation accuracy. For the short lane experiment, the BOQ MAE for the ACTM with and without the proposed short lane extension is 7 m and 25 m, respectively, whereas for the CTM it is 24 m.

c) The proposed extension for the shared lane enhances the capacity of the CTM to realistically model the shared lane where its queue discharge process is frequently interrupted by opposing vehicles, resulting in a non-continuous discharge process. The BOQ for shared lanes is estimated with a MAE of 18 m.

d) The proposed extension for balancing lane utilisation enhances the BOQ estimation accuracy by 50% for sites with an unbalanced lane utilisation. The BOQ MAE for the ACTM with and without lane utilisation balancing is 20 m and 47 m, respectively, whereas for the CTM it is 52 m.

e) The extensions introduced in the ACTM for improving its accuracy and scope, slightly (approximately by 15%) increases its computation time compared to the traditional CTM. However, this increase will not be proportional to the size of the network as each link will not need the aforementioned extensions.

The improved accuracy in the estimation of the BOQ enhances the applicability of the ACTM for signal optimisation, incorporating the BOQ in the objective function, and subsequently, considering the impact of spillbacks and blockages. This should also improve the effectiveness of the offset optimisation using the ACTM (offset is a function of the queue length). Furthermore, the ability of the ACTM to model the lane interactions should enhance the signal optimisation results as it can correctly analyse the delay due to spillbacks or blockages from the short lane and the shared lane. A future extension could be the utilisation of the ACTM in an optimisation model for the design of an arterial signal, and to propose an effective online signal optimisation algorithm. In Shirke et al. (2018), we have presented the initial results from the ACTM application for the design of robust signal timings.

In this paper, the proposed model is validated on limited real data on an arterial link between two signalised intersections. To thoroughly test the efficacy of the ACTM in the real-world scenarios, it should be validated further with data from different sites, including an arterial corridor or network with various lane configurations.

Acknowledgements

References

Adacher, L., & Tiriolo, M. (2018). A macroscopic model with the advantages of microscopic model: A review of Cell Transmission Model's extensions for urban traffic networks. *Simulation Modelling Practice and Theory*.

Akcelik, R. (1988). *Capacity of a shared lane.* Paper presented at the Australian Road Research Board Proceedings.

Akcelik, R. (1989). Opposed turns at signalized intersections: the Australian method. *ITE journal, 59*(6), 21-27.

Akçelik, R. (1997). Lane-by-lane modelling of unequal lane use and flares at roundabouts and signalised intersections: the SIDRA solution. *Traffic Engineering+ Control, 38*(7), 388-399.

Akçelik, R., Besley, M., & Roper, R. (1999). *Fundamental relationships for traffic flows at signalised intersections*.

Alecsandru, C., Quddus, A., Huang, K. C., Rouhieh, B., Khan, A. R., & Zeng, Q. (2011). *An assessment of the cell-transmission traffic flow paradigm: Development and applications.* Paper presented at the Transportation Research Board 90th Annual Meeting.

Alecsandru, C. D. (2006). *A stochastic mesoscopic cell-transmission model for operational analysis of large-scale transportation networks.* (Ph. D. thesis).

Avram, C., & Boel, R. (2005). Distributed implementation of a heterogeneous simulation of urban road traffic. *SIMULATION IN WIDER EUROPE*, 833-840.

Binning, J. C., Burtenshaw, G., & Crabtree, M. (2009). TRANSYT 13 User Guide. *TRL Software, Crowthorne, Berkshire, UK*.

Boel, R., & Mihaylova, L. (2006). A compositional stochastic model for real time freeway traffic simulation. *Transportation Research Part B: Methodological, 40*(4), 319-334.

Canudas-de-Wit, C., & Ferrara, A. (2018). A variable-length Cell Transmission Model for road traffic systems. *Transportation Research Part C: Emerging Technologies, 97*, 428-455. doi:https://doi.org/10.1016/j.trc.2018.07.023

Carey, M., Balijepalli, C., & Watling, D. (2015). Extending the cell transmission model to multiple lanes and lane-changing. *Networks and Spatial Economics, 15*(3), 507-535.

Casas, J., Ferrer, J. L., Garcia, D., Perarnau, J., & Torday, A. (2010). Traffic simulation with aimsun *Fundamentals of traffic simulation* (pp. 173-232): Springer.

Celikoglu, H. B. (2014). Dynamic classification of traffic flow patterns simulated by a switching multimode discrete cell transmission model. *IEEE Transactions on Intelligent transportation systems, 15*(6), 2539-2550.

Celikoglu, H. B., & Silgu, M. A. (2016). Extension of traffic flow pattern dynamic classification by a macroscopic model using multivariate clustering. *Transportation science, 50*(3), 966-981.

Chen, C., Hu, J., & Wang, Y. (2010a). *Cell-based simulation and estimation of urban traffic network.* Paper presented at the 13th International IEEE Conference on Intelligent Transportation Systems.

Chen, P., Qi, H., & Sun, J. (2014). Investigation of Saturation Flow on Shared Right-Turn Lane at Signalized Intersections. *Transportation Research Record: Journal of the Transportation Research Board*(2461), 66-75.

Chen, X., Shi, Q., & Li, L. (2010b). Location specific cell transmission model for freeway traffic. *Tsinghua Science and Technology, 15*(4), 475-480.

Chow, A. H., & Lo, H. K. (2007). Sensitivity analysis of signal control with physical queuing: Delay derivatives and an application. *Transportation Research Part B: Methodological, 41*(4), 462-477.

Creasey, F., Stamatiadis, N., & Viele, K. (2011). Right-turn-on-red volume estimation and incremental capacity models for shared lanes at signalized intersections. *Transportation Research Record: Journal of the Transportation Research Board*(2257), 31-39.

Daganzo, C. F. (1994). The cell transmission model: A dynamic representation of highway traffic consistent with the hydrodynamic theory. *Transportation Research Part B: Methodological, 28*(4), 269-287.

Daganzo, C. F. (1995). The cell transmission model, part II: network traffic. *Transportation Research Part B: Methodological, 29*(2), 79-93.

Daganzo, C. F. (1999). The lagged cell-transmission model.

Gao, Y., Liu, Y., Hu, H., & Ge, Y. e. (2016). Modeling traffic operation at signalized intersections without explicit left-turn yielding rules with an enhanced cell transmission model. *Journal of Advanced Transportation, 50*(7), 1470-1488.

Hadfi, R., Tokuda, S., & Ito, T. (2017). Traffic simulation in urban networks using stochastic cell transmission model. *Computational Intelligence, 33*(4), 826-842.

Han, Y., Hegyi, A., Yuan, Y., Hoogendoorn, S., Papageorgiou, M., & Roncoli, C. (2017). Resolving freeway jam waves by discrete first-order model-based predictive control of variable speed limits. *Transportation Research Part C: Emerging Technologies, 77*, 405-420.

Han, Y., Yuan, Y., Hegyi, A., & Hoogendoorn, S. P. (2016). New extended discrete first-order model to reproduce propagation of jam waves. *Transportation Research Record: Journal of the Transportation Research Board*(2560), 108-118.

Horiguchi, R., Katakura, M., Akahane, H., & Kuwahara, M. (1994, 1994). *A development of a traffic simulator for urban road networks: AVENUE.* Paper presented at the 5th Vehicle Navigation & Information Systems Conference Yokohama, Japan.

Iryo-Asano, M., Sumalee, A., Kuwahara, M., & Tanaka, S. (2007). *Dynamic Cell Transmission-Based Pedestrian Model with Multidirectional Flows and Strategic Route Choices* (Vol. 2039).

Kays, H. I., Shimu, T. H., Hadiuzzaman, M., Muniruzzaman, S. M., & Mizanur Rahman, M. (2017). H-CTM for simulating non-lane-based heterogeneous traffic. *Transportation Letters*, 1-9.

Kurzhanskiy, A., Kwon, J., & Varaiya, P. (2008). Aurora—Object-Oriented Framework for Simulation and Analysis of Flow Networks. *Tools for Operational Planning Project, California PATH*.

Laval, J. A., & Daganzo, C. F. (2006). Lane-changing in traffic streams. *Transportation Research Part B: Methodological, 40*(3), 251-264. doi:h[ttp://dx.doi.org/10.1016/j.trb.2005.04.003](http://dx.doi.org/10.1016/j.trb.2005.04.003)

Levin, M. W., & Boyles, S. D. (2016a). A cell transmission model for dynamic lane reversal with autonomous vehicles. *Transportation Research Part C: Emerging Technologies, 68*, 126-143.

Levin, M. W., & Boyles, S. D. (2016b). A multiclass cell transmission model for shared human and autonomous vehicle roads. *Transportation Research Part C: Emerging Technologies, 62*, 103-116.

Li, Z. (2010). Modeling arterial signal optimization with enhanced cell transmission formulations. *Journal of Transportation Engineering, 137*(7), 445-454.

Lighthill, M. J., & Whitham, G. B. (1955). *On kinematic waves. II. A theory of traffic flow on long crowded roads.* Paper presented at the Proceedings of the Royal Society of London A: Mathematical, Physical and Engineering Sciences.

Lin, W.-H., & Wang, C. (2004). An enhanced 0-1 mixed-integer LP formulation for traffic signal control. *IEEE Transactions on Intelligent transportation systems, 5*(4), 238-245.

Liu, H., Wang, J., Wijayaratna, K., Dixit, V. V., & Waller, S. T. (2015). Integrating the bus vehicle class into the cell transmission model. *IEEE Transactions on Intelligent transportation systems, 16*(5), 2620-2630.

Liu, Y., & Chang, G.-L. (2011). An arterial signal optimization model for intersections experiencing queue spillback and lane blockage. *Transportation Research Part C: Emerging Technologies, 19*(1), 130-144.

Lo, H. (2001). A cell-based traffic control formulation: strategies and benefits of dynamic timing plans. *Transportation science, 35*(2), 148-164.

Lo, H. K., Chang, E., & Chan, Y. C. (2001). Dynamic network traffic control. *Transportation Research Part A: Policy and Practice, 35*(8), 721-744.

Lo, H. K., & Szeto, W. Y. (2002). A cell-based variational inequality formulation of the dynamic user optimal assignment problem. *Transportation Research Part B: Methodological, 36*(5), 421-443. doi:https://doi.org/10.1016/S0191-2615(01)00011-X

Long, J., Gao, Z., Zhao, X., Lian, A., & Orenstein, P. (2011). Urban traffic jam simulation based on the cell transmission model. *Networks and Spatial Economics, 11*(1), 43-64.

Lu, S., Dai, S., & Liu, X. (2011). A discrete traffic kinetic model–integrating the lagged cell transmission and continuous traffic kinetic models. *Transportation Research Part C: Emerging Technologies, 19*(2), 196-205.

Muñoz, L., Sun, X., Horowitz, R., & Alvarez, L. (2003). *Traffic density estimation with the cell transmission model.* Paper presented at the Proceedings of the 2003 American Control Conference, 2003.

Richards, P. I. (1956). Shock waves on the highway. *Operations research, 4*(1), 42-51.

Roncoli, C., Papageorgiou, M., & Papamichail, I. (2015). Traffic flow optimisation in presence of vehicle automation and communication systems–Part I: A first-order multi-lane model for motorway traffic. *Transportation Research Part C: Emerging Technologies, 57*, 241-259.

Shirke , C., Sabar, N., Chung, E., & Bhaskar, A. (2018). *Design of Robust Signal Timings for arterial traffic variations using macroscopic simulation*. Paper presented at the ISTS & IWTDCS 2018, Matsuyama, Japan.

Srivastava, A., Jin, W.-L., & Lebacque, J.-P. (2015). A modified Cell Transmission Model with realistic queue discharge features at signalized intersections. *Transportation Research Part B: Methodological, 81, Part 1*, 302-315. doi:http://dx.doi.org/10.1016/j.trb.2015.05.013

Su, D., Kurzhanskiy, A., & Horowitz, R. (2013). *Simulation of Arterial Traffic Using Cell Transmission Model.* Paper presented at the 92nd Transportation Research Board Annual Meeting.

Sumalee, A., Zhong, R. X., Pan, T. L., & Szeto, W. Y. (2011). Stochastic cell transmission model (SCTM): A stochastic dynamic traffic model for traffic state surveillance and assignment. *Transportation Research Part B: Methodological, 45*(3), 507-533. doi:https://doi.org/10.1016/j.trb.2010.09.006

Sun, D., & Elefteriadou, L. (2012). A driver behavior-based lane-changing model for urban arterial streets. *Transportation science, 48*(2), 184-205.

Szeto, W., Ghosh, B., Basu, B., & O'Mahony, M. (2009). Multivariate traffic forecasting technique using cell transmission model and SARIMA model. *Journal of Transportation Engineering, 135*(9), 658-667.

Szeto, W. Y. (2008). Enhanced Lagged Cell-Transmission Model for Dynamic Traffic Assignment. *2085*(1), 76-85. doi:10.3141/2085-09

Szeto, W. Y., & Lo, H. K. (2004). A cell-based simultaneous route and departure time choice model with elastic demand. *Transportation Research Part B: Methodological, 38*(7), 593-612. doi:https://doi.org/10.1016/j.trb.2003.05.001

Tajtehranifard, H., Bhaskar, A., Haque, M. M., Nassir, N., & Chung, E. (2017). *System Optimal Quasi-Dynamic Traffic Assignment with Application in Incident Traffic Re-Routing*. Paper presented at the The 96th Annual Meeting of the Transportation Research Board.

Tiaprasert, K., Zhang, Y., Aswakul, C., Jiao, J., & Ye, X. (2017). Closed-form multiclass cell transmission model enhanced with overtaking, lane-changing, and first-in first-out properties. *Transportation Research Part C: Emerging Technologies, 85*, 86-110. doi:hhttps://doi.org/10.1016/j.trc.2017.09.008

Tokuda, S., Kanamori, R., & Ito, T. (2017). A Modification of the Stochastic Cell Transmission Model for Urban Networks. *International Journal of Intelligent Transportation Systems Research, 15*(2), 73-84.

Tuerprasert, K., & Aswakul, C. (2010). Multiclass cell transmission model for heterogeneous mobility in general topology of road network. *Journal of Intelligent Transportation Systems, 14*(2), 68-82.

Van den Berg, M., Hegyi, A., De Schutter, B., & Hellendoorn, H. (2007). Integrated traffic control for mixed urban and freeway networks: A model predictive control approach. *European journal of transport infrastructure research, 7*(3).

Wang, P., Jones, L., & Yang, Q. (2012). A novel conditional cell transmission model for oversaturated arterials. *Journal of Central South University, 19*(5), 1466-1474.

Webster, F. V. (1958). *Traffic signal settings*. Retrieved from

Work, D. B., Tossavainen, O.-P., Blandin, S., Bayen, A. M., Iwuchukwu, T., & Tracton, K. (2008). *An ensemble Kalman filtering approach to highway traffic estimation using GPS enabled mobile devices*. Paper presented at the 2008 47th IEEE Conference on Decision and Control.

Wu, N. (2011). Modelling blockage probability and capacity of shared lanes at signalized intersections. *Procedia-Social and Behavioral Sciences, 16*, 481-491.

Xie, B., Xu, M., Härri, J., & Chen, Y. (2013). *A traffic light extension to Cell Transmission Model for estimating urban traffic jam*. Paper presented at the 2013 IEEE 24th Annual International Symposium on Personal, Indoor, and Mobile Radio Communications (PIMRC).

Xu, J., Yang, X., & Lao, Y. (2008). *Study on the capacity of left-through shared lane with permitted left-turn phasing*. Paper presented at the Intelligent Computation Technology and Automation (ICICTA), 2008 International Conference on.

Xu, Y., Kong, Q., Lin, S., & Liu, Y. (2012, 11-14 April 2012). *Urban traffic flow prediction based on road network model*. Paper presented at the Proceedings of 2012 9th IEEE International Conference on Networking, Sensing and Control.

Zhang, H., Nie, Y., & Qian, Z. (2013). Modelling network flow with and without link interactions: the cases of point queue, spatial queue and cell transmission model. *Transportmetrica B: Transport Dynamics, 1*(1), 33-51.

Zhang, Z., Wolshon, B., & Dixit, V. V. (2015). Integration of a cell transmission model and macroscopic fundamental diagram: Network aggregation for dynamic traffic models. *Transportation Research Part C: Emerging Technologies, 55*, 298-309. doi:https://doi.org/10.1016/j.trc.2015.03.040

Zhong, R., & Sumalee, A. (2008). Stochastic cell transmission model: traffic state estimation under uncertainties *Traffic and Transportation Studies* (pp. 462-478).

Zhou, Y., & Zhuang, H. (2011). Traffic performance in signalized intersection with shared lane and left-turn waiting area established. *Journal of Transportation Engineering, 138*(7), 852-862.

Ziliaskopoulos, A., & Lee, S. (1996). A cell transmission based assignment-simulation model for integrated freeway/surface street systems. *Transportation Research Record, 1701*, 12-23.

Ziliaskopoulos, A. K., & Waller, S. T. (2000). An Internet-based geographic information system that integrates data, models and users for transportation applications. *Transportation Research Part C: Emerging Technologies, 8*(1), 427-444.